NASA TECHNICAL NOTE

NASA TN D-7581

NASA TN D-7581

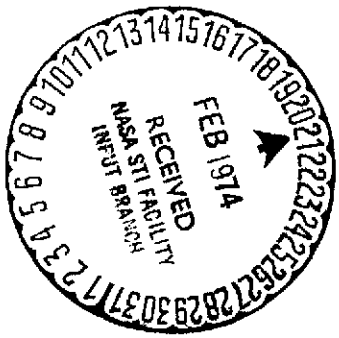

EXPLORATORY TESTS OF TWO STRUT FUEL INJECTORS FOR SUPERSONIC COMBUSTION

by Griffin Y. Anderson and Paul B. Gooderum

Langley Research Center

Hampton, Va. 23665

NATIONAL AERONAUTICS AND SPACE ADMINISTRATION • WASHINGTON, D. C. • FEBRUARY 1974

1. Report No.	2. Government Accession No.	3. Recipient's Catalog No.
NASA TN D-7581		

4. Title and Subtitle	5. Report Date
EXPLORATORY TESTS OF TWO STRUT FUEL INJECTORS FOR SUPERSONIC COMBUSTION	February 1974
	6. Performing Organization Code

7. Author(s)	8. Performing Organization Report No.
Griffin Y. Anderson and Paul B. Gooderum	L-9428
	10. Work Unit No. 501-04-03-02
9. Performing Organization Name and Address	11. Contract or Grant No.
NASA Langley Research Center Hampton, Va. 23665	
	13. Type of Report and Period Covered
12. Sponsoring Agency Name and Address	Technical Note
National Aeronautics and Space Administration Washington, D.C. 20546	14. Sponsoring Agency Code

15. Supplementary Notes

16. Abstract

Results of supersonic mixing and combustion tests performed with two simple strut injector configurations, one with parallel injectors and one with perpendicular injectors, are presented and analyzed. Good agreement is obtained between static pressure measured on the duct wall downstream of the strut injectors and distributions obtained from one-dimensional calculations. Measured duct heat load agrees with results of the one-dimensional calculations for moderate amounts of reaction but is underestimated when large separated regions occur near the injection location. For the parallel injection strut, good agreement is obtained between the shape of the injected fuel distribution inferred from gas sample measurements at the duct exit and the distribution calculated with a multiple-jet mixing theory. The overall fraction of injected fuel reacted in the multiple-jet calculation closely matches the amount of fuel reaction necessary to match static pressure with the one-dimensional calculation. Gas sample measurements with the perpendicular injection strut also give results consistent with the amount of fuel reaction in the one-dimensional calculation.

17. Key Words (Suggested by Author(s))	18. Distribution Statement
Supersonic combustion Scramjet Fuel injectors	Unclassified – Unlimited STAR Category 28

19. Security Classif. (of this report)	20. Security Classif. (of this page)	21. No. of Pages	22. Price*
Unclassified	Unclassified	~~46~~ 49	$3.00

*For sale by the National Technical Information Service, Springfield, Virginia 22151

EXPLORATORY TESTS OF TWO STRUT FUEL INJECTORS FOR SUPERSONIC COMBUSTION

By Griffin Y. Anderson and Paul B. Gooderum
Langley Research Center

SUMMARY

Results of supersonic mixing and combustion tests performed with two simple strut injector configurations, one with parallel injectors and one with perpendicular injectors, are presented and analyzed. Good agreement is obtained between static pressure measured on the duct wall downstream of the strut injectors and distributions obtained from one-dimensional calculations. Measured duct heat load agrees with results of the one-dimensional calculations for moderate amounts of reaction but is underestimated when large separated regions occur near the injection location. For the parallel injection strut, good agreement is obtained between the shape of the injected fuel distribution inferred from gas sample measurements at the duct exit and the distribution calculated with a multiple-jet mixing theory. The overall fraction of injected fuel reacted in the multiple-jet calculation closely matches the amount of fuel reaction necessary to match static pressure with the one-dimensional calculation. Gas sample measurements with the perpendicular injection strut also give results consistent with the amount of fuel reaction in the one-dimensional calculation.

INTRODUCTION

The feasibility and performance potential of the supersonic combustion ramjet (scramjet) engine for flight at hypersonic speeds was firmly established by a number of successful research-scale engine demonstrations in the 1960's. (See ref. 1 for discussion.) The particular configurations and internal aerothermodynamic design features that will eventually evolve for practical flight applications are only now beginning to emerge. The importance of carefully integrating the engine with the vehicle and of reducing engine cooling requirements is emphasized by results in references 2 and 3. Low engine cooling load is necessary to maintain an engine fuel cooling margin that can be used for active cooling of parts of the vehicle other than the engine. Since the combustor can account for 60 percent to 80 percent of the engine cooling requirement, reduced cooling is a first-order consideration in supersonic combustor design.

Most of the research-scale engine work relied entirely on flush wall fuel injectors in their combustor designs. (See ref. 1.) As the combustor length is a function of the combustor height at the point of fuel injection, instream fuel injection from struts in multiple planes provides a direct means for reducing the combustor length and cooling requirement for full-scale engines. Reference 4 reports results of tests with a large circular supersonic combustor (46-cm diameter) in which various strut fuel injector designs and arrangements were explored. However, in that study the struts are intended only as fuel injectors; strut blockage and drag are considered to be performance penalties. The integrated scramjet engine concept discussed in references 2, 3, and 5 is based on an inlet which employs multiple swept struts with carefully designed upstream contours to perform the bulk of the inlet compression process. In fact, as pointed out in reference 5, the struts may block about 60 percent of the flow cross-sectional area in the throat (minimum cross-sectional area) region of the inlet. Although this blockage produces drag, the drag is a necessary part of the inlet compression process and is not a fuel injector loss. Fuel injectors can then be designed into the aft part of the inlet compression struts to achieve a short combustor. As pointed out in reference 5, injection both parallel to and perpendicular to the oncoming flow direction may be desirable to achieve the best performance from a particular combustor geometry at different flight speeds.

The principal objective of the present study is to determine the flow fields produced by simple strut injectors and attempt to model those flow fields by comparison of test data with results calculated by using a one-dimensional analysis and empirical mixing models. The emphasis in the experimental design is to achieve representative strut injector flow fields (rather than model a particular engine configuration) with minimum hardware complexity and maximum use of existing supersonic combustor hardware. For this reason, the injector struts are oriented perpendicular to the flow direction (without leading-edge sweep). Although this orientation greatly simplifies the experimental design, it must be recognized that cross flow and other effects will occur with swept injection struts which may be important in an engine design; further experiments will be required to assess the importance of the effects of sweep on the mixing reacting flow field generated by strut injection.

Tests are conducted at conditions simulating Mach 7 flight with parallel and perpendicular injection struts in three test configurations: free jet, short duct, and long duct. The free-jet tests are intended to determine the adequacy of the mechanical and thermal design of the struts, give a qualitative picture of the flow field, and allow some cut-and-try modification of the injector port designs. The short-duct tests are used to verify starting of the ducted configuration. The long-duct tests are designed to provide enough measurements to determine combustion performance. Wall static pressure and duct

cooling requirements are measured along with duct exit probe measurements of pitot pressure and gas composition.

SYMBOLS

c_1, c_2 correlation parameters (see eq. 2)

d injector diameter

f burner fuel to oxidizer ratio, $\frac{\text{Fuel flow}}{\text{Air + oxygen flow}}$

I burner free oxygen parameter, $\frac{\text{(Oxygen flow) (0.0823)}}{\text{Fuel flow}}$; for I = 1, test gas has same free oxygen content as air (20.95 percent by volume)

M Mach number

p pressure

p_a ambient pressure

Q duct heat load

Q_o duct heat load with no fuel injection

q_r ratio of jet pressure to stream dynamic pressure

s jet spacing

T temperature

x distance measured in flow direction

x_ℓ length for complete reaction of injected fuel

y distance measured across long dimension of duct from the duct center line

y' shifted coordinate defined as the distance measured across long dimension of duct from the nearest jet center line

z	distance measured across short dimension of duct from center line
α	local mass fraction of injected fuel
α_{bulk}	bulk mass fraction of injected fuel, $\frac{\omega_j}{\omega_h + \omega_j}$
β	short duct angular misalinement (see figs. 9 and 10)
η_c	combustion efficiency, $\frac{\phi_r}{\phi}$
ϕ	injected equivalence ratio
ϕ_r	reacted equivalence ratio
ω	mass flow rate

Subscripts:

e	duct exit
h	burner
j	injector
T	stagnation
2	pitot

ANALYSIS

The ability to calculate the wall pressure distribution and heat transfer that occur in a supersonic combustor is important for the evaluation of any proposed scramjet engine design. The general problem is very complex, and involves supersonic flow, fuel injection, turbulent mixing, and combustion; as a first step, a simplified analysis is desirable. One approach to developing a simplified analysis is described in the following paragraphs. The theory is one dimensional and includes the effects of area change, wall friction, heat transfer, fuel injection and reaction, but does not include shock waves, flow separation, or chemical kinetic effects.

One-Dimensional Flow Model

A schematic of the supersonic combustion flow model used for calculations in this report is shown in figure 1. The analysis is based on the one-dimensional conservation equations for mass, momentum, and energy. Independent input parameters to the analysis are the geometry of the combustor, entering flow conditions, fuel injection distribution, fuel reaction distribution, wall skin-friction coefficient, and wall temperature as indicated in figure 1. With these parameters given, the conservation equations are used to calculate the flow properties along the combustor, stepwise, in a marching procedure starting from the combustor entrance. Thus, the calculation provides flow properties and wall heat-transfer distributions with axial distance along the combustor. The computer program (LAR-11041) which is used to make the calculations is available from COSMIC (University of Georgia).

Gas model.- Gas properties are calculated in the computer program by using tabulated real-gas thermodynamic properties and allowing for up to nine chemical species (H_2O, O_2, H_2, N_2, Ar, O, H, NO, and OH). The amount of each species present is determined from a chemical equilibrium calculation which has a partial reaction feature. Equilibrium chemical composition is calculated for the combustion products of the test gas and reacted fuel at a given axial location. Any fuel injected but remaining unreacted at that location is kept in thermal equilibrium with these combustion products.

Fuel reaction distribution.- Specification of an appropriate fuel reaction distribution with length for a given combustor geometry and fuel injector design is the key problem in using the analysis. If the static temperature and pressure of the flow are high so that local chemical equilibrium can be assumed, then the amount of fuel reaction with length is the same as the amount of accomplished fuel mixing with length. This approach is used successfully in references 5 and 6 to model supersonic combustion flow fields with parallel and perpendicular fuel injection.

In reference 6 parallel injection with a single jet in a coaxial supersonic mixing and combustion experiment is found to produce a nearly linear variation of accomplished mixing and combustion with length from the injector. Thus,

$$\eta_c = \frac{\phi_r}{\phi} = \frac{x}{x_\ell} \tag{1}$$

where x_ℓ is defined as the length for complete mixing or reaction. The value of x_ℓ is estimated from mixing theory such as the analysis described in reference 7. For such an estimate an appropriate eddy viscosity model is required. The eddy viscosity model developed in reference 8 with a value of empirical constant in the model equal to 0.01 is used successfully in reference 6 to correlate both reacting and nonreacting data. Refer-

ence 9 presents an analysis for multiple parallel jets with merging mixing patterns, but empirical turbulent transport rates or eddy viscosity models have not been developed for this analysis.

Analyses (equivalent to those of refs. 7 and 9 for parallel injection) are not available for perpendicular injection flow fields. The study in reference 10 provides a direct empirical approach to representing the accomplished mixing in perpendicular injection flow fields. Reference 10 reports extensive composition profile data for multijet perpendicular wall injection of hydrogen in air without reaction. Integrations of the profile data were used to determine the amount of accomplished mixing defined at any downstream location as the fraction of injected fuel that would react if complete reaction occurred without further mixing. The correlations of these results presented in reference 10 were used in reference 5 to determine a schedule of reaction with distance from the injection point shown in table I. This schedule of reaction was used successfully in reference 5 to model wall static-pressure data from a supersonic combustion experiment with perpendicular wall injection. The value of length for complete mixing x_ℓ is calculated from

$$x_\ell = c_1 d\left(q_r\right)^{c_2} \tag{2}$$

where d is the injector diameter and c_1 and c_2 are parameters from the correlations of reference 10 that depend on injector spacing.

TABLE I.- DIMENSIONLESS REACTION DISTRIBUTION FOR PERPENDICULAR INJECTION

ϕ_r/ϕ	x/x_ℓ
0	0
.19	.01
.75	.20
.85	.40
.94	.70
1.00	1.00

Application

The analytical approach described in the preceding paragraphs depends entirely on the specification of an appropriate fuel reaction distribution with length for the supersonic combustor geometry and fuel injector design of interest. Representative dimensionless reaction distributions have been indicated for parallel injection (eq. (1)) and

perpendicular injection (table I) along with means of estimating the length required for complete mixing. With these distributions as a guide, the analysis can be used to calculate wall static-pressure distribution and heat transfer for a particular supersonic combustion experiment. If the reaction distribution specified is appropriate for that particular test, then calculated wall pressure should fit measured data at least where pressure changes due to heat release and area change dominate. Thus, the calculated results must match wall pressure data closely in diverging parts of a combustion duct, but might depart considerably from the data in regions with shock waves or separated flow such as regions near perpendicular fuel injection.

In addition to matching wall pressure, the calculated results must also agree with any other measured flow quantities that can be obtained from the experiment. Thus, heat transfer, instream pitot pressure, gas composition, and other information available from a particular experiment should be compared with the calculated results. If agreement of several sets of measurements can be demonstrated, then the reaction distribution used for the calculation can be considered to be appropriate; and evidence to support its use in making other supersonic combustion calculations for similar conditions has been established. In effect, as used in this report, the simplified analysis described serves as a correlating tool to show the consistency or lack of consistency of different kinds of measurements obtained from the same experiment. If agreement between calculations and data can be demonstrated for a range of geometries, injector designs, and conditions, then support is provided for using the analysis as a design tool.

APPARATUS AND PROCEDURE

Test gas for the experiments is provided by a hydrogen-oxygen-air burner shown in figure 2. The gases are supplied at high pressure in controlled proportions to a water-cooled chamber where they mix and burn. Details of the burner, its operation, and performance are contained in reference 11. For reacting tests the burner is controlled to supply oxygen-replenished combustion products containing approximately 21 percent oxygen, 46 percent nitrogen, and 33 percent water by volume with a stagnation temperature of about 2050 K; for nonreacting tests the burner supplies stoichiometric hydrogen-air combustion products containing approximately 65 percent nitrogen and 35 percent water with a stagnation temperature of 2200 K. The test gas is expanded through a two-dimensional contoured supersonic nozzle to a nominal Mach number of 2.7. Unpublished pitot and gas sample surveys of the nozzle exit plane for oxygen-replenished test gas and a burner pressure of 2 MN/m^2 show the Mach number to be 2.70 ± 0.05 and show less than ±5 percent variation in the local concentration of burner fuel. This level of variation in burner fuel concentration implies a variation in local stagnation temperature of less than ±75 K.

The strut injectors are mounted on the center line of the nozzle spanning the longer dimension. Three types of tests were conducted: (1) tests in the free-jet produced by the nozzle (fig. 2); (2) tests in a short water-cooled duct section that extends approximately 3 cm downstream of the injection location (fig. 3); and (3) tests with an additional long-duct section placed downstream of the short duct (fig. 3). Wall injection studies conducted with this long-duct section are reported in reference 12. For free-jet and short-duct tests, the burner is operated at approximately 3 MN/m^2 which makes the nozzle exit static pressure approximately equal to 1 atmosphere (the ambient pressure of the test cell). For ducted tests the burner is operated at 2 MN/m^2 to reduce heat transfer to the strut.

The strut design and injector details are shown in figure 4. The struts are fabricated of oxygen-free copper by brazing together two halves split by a plane through the axis of the leading edge and parallel to the nozzle-exit flow direction. Hydrogen fuel (at pressures up to 4 MN/m^2) is supplied to the injectors from both ends of the strut in passages that are machined in the halves before brazing. The strut leading edges and the trailing edge of the perpendicular injection strut are tubes which are set in grooves machined in the strut halves and joined to the strut when the halves are brazed. The external wedge contour and injection ports are machined after the halves and tubes are brazed together. In the tests cooling water is supplied to the leading- and trailing-edge tubes at 3.7 MN/m^2 and with flow rates of approximately 0.09 and 0.5 kg/sec, respectively. Most of the strut cooling is supplied by the hydrogen fuel flowing to the injectors so that hydrogen flow is necessary in all tests. The external wedge half-angle of the upstream part of the struts is 6^o which is a "rule of thumb" indicated in reference 5 as the maximum turning angle appropriate for multistrut inlet configurations. The rest of the external shape is largely determined from practical constraints on the design. The maximum strut thickness is 27 percent of the nozzle-exit height to insure starting in the ducted tests. Enough length is added downstream of the maximum thickness to contain the injectors.

The parallel injection strut (fig. 4(a)) has five equally spaced fuel injectors which divide the flow cross section into nearly square regions, each fueled by one jet. The injector throat is sized to allow stoichiometric injection with the maximum fuel supply pressure at the higher test pressure. A conical expansion with 10^o half-angle was chosen arbitrarily to expand the injected fuel in an attempt to match the stream static pressure. After initial free-jet tests one of the injectors was plugged and replaced by two drilled holes as shown in figure 4(a).

The perpendicular injection strut (fig. 4(b)) is provided with a small rearward-facing step at the maximum cross section. The step is intended to isolate the upstream wedge surface from the pressure rise caused by the perpendicular injection and combustion disturbance. Fuel injection is from eight choked holes, four on each side of the strut,

located downstream of the step and equally spaced. This arrangement divides the flow cross section into eight rectangular regions with width (jet spacing) about twice the height. This aspect ratio appears to be appropriate for the injection conditions of the experiment based on the nonreactive mixing results reported in reference 10. The initial hole diameter used is sized to allow stoichiometric injection with the maximum fuel injection pressure at the higher test pressure. Injection hole area was progressively increased in the free-jet tests as shown in the detail in figure 4(b).

Instrumentation for the tests includes flowmetering of all gases supplied to the burner and of the fuel supplied to the strut injector. Burner pressure, duct static pressures, wall temperatures, coolant temperatures, and coolant flow rates are digitized and recorded on magnetic tape by a data acquisition system. Burner operating parameters are available immediately after each test firing to allow on-site evaluation of test success and to guide the choice of succeeding test parameters.

Pitot pressure and gas sample measurements are made 5.3 cm downstream of the duct exit with the water-cooled nine-probe rake shown schematically in figure 5. Each probe has a 20° half-angle conical tip with a passage on the center line for pitot-pressure measurement and gas-sample withdrawal. The passage has a diameter of 0.079 cm at the tip and has a 4° half-angle expansion inside the tip which increases the diameter to 0.155 cm. This internal-area increase is intended to reduce the shock-wave strength ahead of the probe tip during sample acquisition. Gas samples are collected in 75-cm^3 stainless steel bottles, and a gas chromatograph is used to determine the relative amount of H_2, O_2, and N_2 in each sample on a dry basis. The instream (wet) sample composition and the local mass fraction of injected fuel are calculated with a mass balance from the dry sample composition and the measured gas flow rates supplied to the burner. Details of the probe, sample acquisition, and analysis techniques are presented in reference 12.

The test conditions are established by presetting supply pressures for air, hydrogen, and oxygen to the test gas burner and for hydrogen fuel to the strut injector. Cooling water flows to the burner, strut, and probe rake are started. The test sequence consists of starting fuel flow to the strut injectors, lighting the burner, recording data, and operating the probe rake. In the free-jet and short-duct tests where the probe rake is not used, burner firings of about 10 seconds are adequate to achieve steady test conditions and acquire data; in the long-duct tests where the probe rake is used, 15-second burner firings are required. For pitot pressure measurement the rake traverse mechanism is stopped to obtain a steady reading at five positions in the duct exit in a single burner firing. For gas sample acquisition, the rake is moved to a single location near the center of the duct exit. Pitot pressure is recorded and then the sample cylinders are filled to approximately 40 percent of the local pitot pressure.

RESULTS AND DISCUSSION

Results from tests of the parallel and perpendicular injection strut fuel injectors in the free-jet, short-duct, and long-duct configurations are discussed and analyzed in the following sections.

Free-Jet Tests

Leading-edge survival.- The initial leading-edge diameter for both struts was 0.16 cm or about half the leading-edge coolant tube outside diameter. With this diameter the leading edge was a thin section brazed to the front of the coolant tube and survived only a few preliminary hot test firings without damage. It failed completely in a test at burner conditions of 2.3 MN/m^2 and 2200 K. The diameter was increased to 0.24 cm by removing material from the leading edge of the second strut for its first test. Under similar test conditions the leading edge again failed completely. The leading edges of both struts were machined to 0.32 cm diameter so that the coolant tube surface was exposed and the tube became the leading edge. No further difficulties occurred with the strut leading edges. Apparently, the braze joint between the coolant tube and leading-edge material upstream of the tube gave poor thermal contact which resulted in high-temperature differences for the heat-flux levels of the tests. Once material temperatures rose sufficiently to allow braze alloy melting, aerodynamic loading separated the leading-edge halves; the material no longer in contact with the coolant tube quickly burned away.

Strut heat load.- Measured heat transfer to the perpendicular injection strut is shown in figure 6 plotted against the product of burner pressure and fuel to oxidizer ratio (f is approximately proportional to test gas stagnation temperature). The heat transfer to the leading and trailing edge is calculated from coolant flow rate and measured temperature rise. The fuel temperature increase at the injectors and heat transfer to the fuel are estimated (when the injectors are assumed to be choked) from the pressure required to supply a given flow of fuel to the strut in the hot firing test compared with the pressure required for the same fuel flow cold and without the burner firing. Thus,

$$T_{hot} - T_{cold} = T_{cold}\left[\left(\frac{p_{hot}}{p_{cold}}\right)^2 - 1\right] \tag{3}$$

Trend lines through the origin are shown for each group of data points. Note that the trailing-edge heat load is nearly twice the heat load for the leading edge. Since the trailing-edge diameter is twice the final diameter of the leading edge, this result implies nearly equal average heat flux to the leading and trailing edges. The fuel to the strut

injectors absorbs about twice the heat load of the trailing edge. The heat load to the leading edge is no different for runs in reacting and nonreacting flow, but the heat loads for the fuel and trailing edge are higher for reacting flow as might be expected. No appreciable difference in leading-edge heat load is measured for any of the three leading-edge diameters or for the different injector designs. Consistent fuel heat-transfer results were not obtained for the parallel injection strut because of pressure transducer problems, and only the original (smallest) injector size in the perpendicular injection strut had small enough pressure drop in the fuel supply passages to allow the estimation of heat transfer from supply pressure.

Injector changes.- After initial free-jet tests, one of the injectors on the parallel injection strut was plugged and replaced by two impinging jets with combined area equal to the original injector throat area but at 45° to the flow direction as shown in figure 4(a). This modification was intended to produce more rapid mixing and reaction (and hence brighter emission) than the original injector, but no change in the visible flame pattern was observed. Several changes were made to the injectors on the perpendicular injection strut in order to establish visible emission immediately downstream of the step. In initial free-jet tests a distinct bow wave was visible on each jet downstream of the step and just ahead of each injector. A similarly shaped discoloration of the strut surface (indicating high local heating) was also noted after the tests. Apparently, the flow expanded over the step and reattached to the strut surface before the injection disturbance was encountered. In an engine the base of the step provides thrust, and pressure rise and combustion are desired at the step; therefore, progressive changes were made to move the injection closer to the base of the step. First, injector diameter was increased from 0.32 cm to 0.40 cm; next, additional small holes were added near the base of the step for two of the injectors on one face of the strut. (See fig. 4(b).) This change effectively established visible emission at the step for those two injectors. Finally, the main injection ports were elongated in the direction of the step. The combined effects of moving the injector closer to the step and decreasing injection pressure for a given fuel flow by increasing injector area established visible emission at the step for all injectors. The injector configurations of both the parallel and perpendicular injection struts remained in the form described for the rest of the testing covered in this report.

Short-Duct Tests

Flow photographs.- Photographs of the mixing-reacting flow field produced by the parallel and perpendicular injection struts in the short-duct tests are shown in figures 7 and 8. Since the duct wall reflects the compression wave from the front of the strut as a compression, the pressure near the strut is maintained at a level where emission from the flow can be clearly photographed. In the free-jet tests discussed in the preceding section, good photographs were not obtained although emission patterns similar to those

in the short-duct tests were quite visible to the eye. In the parallel injection flow field (fig. 7), each of the five jets is visible. The fuel-rich jet core appears as a dark streak surrounded by emission from the reacting region. Alternate brighter and darker zones appear in the center of the downstream part of the flow because of waves which originate from a mismatch between duct exit and ambient pressure. The flow field for perpendicular injection (fig. 8) appears brighter than the parallel injection flow field. Each of the four pairs of injectors produce a burning zone which looks somewhat like the burning zone produced by a parallel jet. The fuel-rich core disappears more quickly in the perpendicular injection strut flow field. The wave structure at the duct exit appears stronger with steeper angle to the flow direction and more change in emission intensity than the parallel injection strut flow field. The mixing-reacting flow fields produced by both injection struts appear steady and no strong shock waves generated by combustion are observed. Perhaps the most striking feature of the flow-field photographs is their orderly appearance with regularly spaced emission zones corresponding to the arrangement of the individual injection ports.

Wall static pressure.- Pressures measured along the center line of one wall of the short-duct section are shown in figures 9 and 10 for the parallel and perpendicular injection strut, respectively. The static pressure near the entrance is slightly above the nominal entrance pressure level $\left(p/p_h = 0.0377\right)$, whereas the pressure near the injection point is slightly less than the level expected following a 6^o compression wave from the upstream section of the strut. The results of simple two-dimensional wave calculations shown by the curves in figures 9 and 10 suggest, as one possibility, that this may be due to a slight misalinement of the duct and the test gas nozzle. If the duct surface where pressure is measured is inclined at a small angle β to the flow leaving the nozzle, initial pressure on the duct wall will be increased by an entrance wave. Also the strength of the strut wedge wave will decrease, and the highest pressure on the wall will occur after the entrance wave reflects from the strut wedge surface and reaches the duct wall. As can be seen in figures 9 and 10, the data are consistent with a misalinement of about 1^o. Although the short-duct wall and the strut were alined by machined surfaces, the duct itself was clamped to the nozzle exit flange against a soft gasket so that a 1^o misalinement is entirely within reason.

For the parallel injection strut (fig. 9), wall pressure near the duct exit is somewhat less than wall pressure opposite the injection location. This result matches the trend expected from the simple wave calculations. The expansion fan from the strut shoulder (where the strut surface turns parallel to the duct wall) tends to reduce wall pressure to nearly the level inside the duct entrance. For the perpendicular injection strut (fig. 10), the wall pressure near the short-duct exit is considerably above the wall pressure opposite the injection location. Apparently, the injection and combustion disturbance produce a compression wave starting near the step on the perpendicular injection strut. It is

interesting to note that varying the fuel flow to the struts from 0.064 to 0.128 kg/sec did not change the measured duct wall pressures. Although this condition corresponds to an increase in fuel flow from roughly half stoichiometric to stoichiometric, apparently the strength of the injection and combustion disturbance for both struts is relatively insensitive to fuel flow.

Long-Duct Tests

The best quantitative description of the flow fields produced by the strut injectors is obtained from the long-duct tests. In the following sections duct static-pressure and heat-transfer data are presented and compared with results calculated with the one-dimensional analysis. Exit probe measurements are also presented and are compared with the one-dimensional calculations and mixing calculations. A list of the test conditions for the runs discussed is included in table II for reference.

TABLE II.- LONG-DUCT TEST CONDITIONS

Run	f	I	p_h, MN/m^2	ω_h, kg/sec	ω_j, kg/sec	$\phi_{(a)}$	Q, MJ/sec	Comments
110- 5	0.031	0	1.83	2.32	0.055	0.70	0.085	Pitot
6								Sample[b]
7	.023	1.12	1.99	2.76	.053	.56	.473	Pitot
8								Sample[b]
10	.026	1.04	1.99	2.62	.053	.59	.268	Pitot
11	.025	1.08	2.02	2.70	.053	.58	.299	Pitot
111- 4	.034	0	1.78	2.20	.060	.80	.14	Pitot
5								Pitot[c]
6	.025	1.07	2.01	2.64	.057	.63	.718	Sample

[a] $\phi \approx \dfrac{\omega_j/\omega_h}{0.034}$

[b]Bad data record. Operating parameters identical to those of previous run. Assume values apply.

[c]Bad data record. Operating parameters identical to those of following run. Assume values apply.

Wall static pressure.- Figures 11 and 12 show wall static-pressure data for the parallel and perpendicular injection struts in nonreacting flow. In each case the data show a pressure rise corresponding to compression waves generated at the front of the strut, followed by varying pressure in the constant area portion after the strut and

smoothly decreasing pressure in the diverging section of the duct. Variations in pressure are larger for the perpendicular injection strut as would be expected because of strong waves and separated regions caused by the injection. Wall pressure computed with the one-dimensional analysis is also shown in the figures. The solid curves represent the computed wall pressure with injection but no reaction for direct comparison with the data. The broken curves represent computed wall pressure without injection. Data are not available to compare with the latter curve since fuel was necessary to cool the strut in all runs. Note that the calculated injection pressure rise is larger for perpendicular injection.

In order to obtain the agreement shown, a total-pressure loss to account for strut drag and shock losses was imposed on the calculations at the injection location. The loss was computed by expanding the flow adiabatically from conditions at the strut shoulder to an assigned static pressure which matches the data in the constant-area section downstream of the strut. This total-pressure loss amounts to about one-half of the burner pressure and is equivalent to a drag coefficient of 0.84 for the strut. The flow conditions are shown in table III. Without this loss the calculated result for no injection would return to the nozzle exit pressure level after the strut; in other words, the analysis would treat the compression and expansion caused by the strut as isentropic.

TABLE III.- INITIAL CONDITIONS FOR ONE-DIMENSIONAL CALCULATIONS

	Nozzle exit	Strut shoulder	Equivalent conditions at injection
Mach number	2.70	2.39	2.11
Area, cm^2	64.74	47.48	64.74
p/p_h	0.0377	0.0616	0.0542
p_T/p_h	1.00	1.00	≈0.5
T/T_T	0.508	0.569	0.632

In figure 13 static-pressure data for parallel injection with reaction are compared with wall pressure computed with the one-dimensional analysis. The equivalent conditions at the injector listed in table III are used to start the calculations. The amount of fuel reacted is computed from equation (1) with the value of x_ℓ equal to 1.16 m. This value of x_ℓ is estimated from calculations made with the computer program described in reference 7 for injection conditions of this experiment and using the turbulent eddy viscosity model developed in reference 8 (with a value of the model constant equal to 0.01). Good agreement between the computed curve and the data is obtained particularly in the diverging part of the duct. The value of x_ℓ in the calculation results in $\eta_c = 0.62$ at

the end of the duct. The data and calculation with reaction lie well above the calculation with no reaction which is shown by the broken curve.

In figure 14 static-pressure data for perpendicular injection with reaction is compared with wall pressure computed by the one-dimensional analysis. The amount of fuel reacted is computed from the values in table I by using linear interpolation. The value of x_ℓ computed from equation (2) is 0.6 m for the injection conditions of this experiment. In contrast to the data for parallel injection (fig. 13), the data in figure 14 for perpendicular injection show a much larger pressure rise near the injectors and in the constant-area part of the duct. In fact, the pressure disturbance caused by the injection and combustion affects some pressure taps in the duct ahead of the injectors. This condition is a result of localized separation of the boundary layer on the duct wall due to the pressure rise. Good agreement between the calculated wall pressure and the data is achieved in the diverging part of the duct. The value of x_ℓ in the calculation results in $\eta_c = 0.85$ at the end of the constant-area section of the duct and $\eta_c = 1$ within the duct at $x = 60$ cm. The data and calculation with reaction lie well above the calculation with no reaction which is shown by the broken curve. Unlike the calculations presented in figures 11 to 13, the calculation with reaction in figure 14 is computed by starting with the isentropic conditions at the strut shoulder; no additional total-pressure loss to account for strut drag and shock losses is included. Apparently, the large amount of heat addition near the injector in the calculation nearly matches the combined heat addition and shock-loss process taking place in the experiment. Duct exit probe measurements discussed in a later section support this conjecture.

Figure 15 presents another set of wall pressure data for the parallel injection strut. Although the hardware and test conditions are identical to those for figure 13, the data are not at all similar. In fact, the data for the parallel injection strut in figure 15 look very similar to the data in figure 14 for the perpendicular injection strut. The calculated curve with reaction presented in figure 14 is included in figure 15 to facilitate comparison. Three test runs subsequent to the test shown in figure 15 produced static-pressure data similar to those of figure 13. Apparently, two different stable flow patterns are possible with the same parallel injection geometry and test conditions. The first (fig. 13) consists of a gradual mixing and reaction process with nearly linear heat release and no strong disturbances. The second (fig. 15) has a strong disturbance at the point of injection and could be modeled by the one-dimensional analysis with a fuel reaction schedule typical of perpendicular injection. This observation implies the existence of a strong recirculating and reacting zone in the strut base region for the data shown in figure 15 but no strong recirculation and reaction immediately behind the strut for the data in figure 13. Reference 13 points out the coupling between combustion-generated pressure rise and shock waves upstream of the fuel injection and combustion, but the dependence of this coupling on the details of the strut geometry and injector design is not known.

Duct heat load.- Water temperature rise and flow rate for the long-duct section downstream of the fuel injection strut were measured in each test, and the duct heat load computed from these quantities is included in table II. Because the water temperature rise is small, there is considerable uncertainty in the duct heat load, particularly for the tests with no reaction. To facilitate comparison of the data, results from a study with the same duct reported in reference 12 are used to nondimensionalize the measured heat loads. In reference 12, the duct heat load with no fuel injection is reported as 0.27 MJ/sec for a ratio of burner fuel to oxidizer of 0.028 and a test-gas flow rate of 3.5 kg/sec. Heat load with no fuel injection for the present study is estimated approximately as

$$Q_O = \left(\frac{\omega_h}{3.5}\right)\left(\frac{f}{0.028}\right)0.27 \text{ MJ/sec} \tag{4}$$

The measured duct heat load nondimensionalized by the estimated heat load with no fuel injection is plotted in figure 16 against the reacted equivalence ratio inferred from the one-dimensional calculations. Duct heat loads for perpendicular wall injection (circular symbols) taken from the study of reference 12 are included for comparison with the strut injection results. Uncertainty of the measured heat load is estimated to be ±0.5 and is evident from the scatter of the nonreacting data. The data for reacted equivalence ratio less than 0.5 agree well with the heat load predicted by the one-dimensional analysis. The calculation is based on a simple Reynolds analogy using a constant skin-friction coefficient of 0.0022 and includes an increase in local heat transfer by a factor of 1.56 in regions of adverse pressure gradient. This increase in local heat transfer to account for the effects of adverse pressure gradient on the boundary layer is derived from unpublished calculations by using the theory of reference 14. For greater amounts of reaction which involve large separated regions near the injector (such as figs. 14 and 15), heat load is above the predicted level. In fact, the measured heat load is of the same order as the level calculated by assuming a local equivalence ratio of stoichiometric at the wall over the entire combustor length.

Pitot-probe measurements.- Figures 17 and 18 present pitot-pressure survey results for the parallel and perpendicular injection struts with injection but no reaction. Measurements near the top and bottom walls, shown by the diamond-shaped symbols, are close enough to the jet boundary to insure that mixing with the ambient air surrounding the jet has reduced the total pressure. Measurements nearer the middle of the jet are significantly higher and show considerable variation. Most of these data are considerably above the pitot pressure corresponding to the one-dimensional calculations shown in figures 11 and 12. Since the duct is overexpanded $\left(p_a/p_e \approx 3.2\right)$, oblique shock waves in the

duct exit reduce the Mach number and increase the pitot pressure seen by the probe tips which are about 5.3 cm downstream of the duct exit. It is interesting that the variation of pitot pressure is somewhat larger for the parallel injection strut (fig. 17) than for the perpendicular injection strut (fig. 18); this result perhaps indicates less uniform fuel distribution for the parallel injection strut. This observation is in qualitative agreement with the amount of reaction needed to match the wall static-pressure data in figures 13 and 14.

Pitot-pressure survey results for the parallel and perpendicular injection struts with reaction are shown in figures 19 and 20, respectively. The range of variation of these data with reaction is much less than the range of variation without reaction shown in figures 17 and 18. Also, the mean of the data appears to be close to the one-dimensional result corresponding to the calculation shown in figures 13 and 14. With reaction the duct exit pressure is much nearer ambient $\left(p_a/p_e \approx 1.4\right)$, and oblique waves at the exit apparently do not affect probe measurements. The pitot-pressure data for the perpendicular injection strut (fig. 20) show much less variation across the short dimension of the duct exit than the data for parallel injection strut (fig. 19). As is the case for the nonreacting data, this result implies more uniform fuel distribution for the perpendicular injection strut and agrees qualitatively with the amount of reaction used in the one-dimensional calculations. (See figs. 13 and 14.)

The filled symbols in figures 17, 19, and 20 show pitot data obtained in runs where gas samples were acquired. In general, these data agree well with data taken in the pitot-pressure survey runs. Figure 21 shows pitot-pressure survey data for the parallel injection strut corresponding to the wall static-pressure distribution shown in figure 15. The data in figure 21 look more like the data obtained with the perpendicular injection strut (fig. 20) than other data obtained with the parallel injection strut (fig. 19). This result agrees with the previously discussed comparison of wall static-pressure data in figures 13 to 15, and supports the conclusion that two different stable flow patterns with different amounts of mixing and heat release exist for the parallel injection strut geometry.

Gas sample measurements.- Results of gas sample measurements for the parallel and perpendicular injection struts are presented in figure 22. All samples were acquired near the horizontal center line of the duct ($z = 0$) and 5.3 cm downstream of the duct exit. Data for the parallel injection strut without reaction (circular symbols) show larger variation than data with reaction (square symbols). Both sets of data for the parallel injection strut show considerably more variation than data with reaction for the perpendicular injection strut (diamond symbols). The peak concentrations in the parallel injection data are well above stoichiometric (which corresponds to about 1.4 on the scale in fig. 22) whereas all the data for perpendicular injection are less than stoichiometric. This condition means that unburned fuel (due to poor fuel distribution) is leaving the duct for parallel injection but not for perpendicular injection. This result agrees with the result

inferred from the comparison of wall static-pressure data and one-dimensional calculations shown in figures 13 and 14. No significant amounts of unreacted hydrogen and oxygen were found together in any single sample. This result implies that there are no very large fluctuations of instantaneous composition from the time-average sample collected in the bottle and is consistent with the partial reaction assumption used in the one-dimensional theory. All the samples show higher fuel concentration than the bulk value except for the end samples which are affected by mixing with ambient air surrounding the duct flow. Higher than average fuel concentration near the center of the duct may be expected, since all fuel is injected from the strut located on the center line.

The parallel injection flow field is predicted by using the mixing theory of reference 9, where mixing and reaction of fuel from multiple parallel jets is computed for a constant value of turbulent eddy viscosity. To apply the theory to the present configuration, the single-jet program of reference 7 was used to calculate the flow field to the point where adjacent jet boundaries merged. The fuel-concentration profiles and the eddy viscosity at that axial location were input to the program of reference 9, and the calculation was continued until the peak concentration was lower than the peak concentration measured with the parallel injection strut. Figures 23 and 24 show that agreement between the data and the theoretical calculations is good. In these figures the data are plotted against distance from the nearest jet center line. A shift of probe location to account for the duct exit shock is used as shown in figure 25. Duct exit flow conditions are taken from the one-dimensional analysis results presented in figures 11 and 13. Note that the location correction only has a large effect on probes 2 and 8 and is larger for the data with no reaction (fig. 23) because the duct flow is more overexpanded with no reaction. Close agreement between symmetrically placed probes in figure 24 indicates the flow field and duct exit shock structure are symmetrical as assumed. In figure 23 symmetry is not as good (compare probes 2 and 8), but the overall match between data and theory is fair when probe location is shifted to account for the exit shock structure.

It should be noted that although the profile agreement in figures 23 and 24 is good, the physical distance downstream of the injector at which the profiles occur in the theoretical calculations does not match the axial-probe location in the experiment. This result reflects the difference between the eddy viscosity value used in the calculation and the effective transport rate in the experiment. An increase in the eddy viscosity for the calculations of about 25 percent is required to match the axial location of the calculated profile in figures 23 and 24 with the axial-probe location. Better turbulence modeling is required to predict the actual concentration decay with length. However, the proper shape profile is predicted, and the overall fraction of fuel burned corresponding to the theoretical profile in figure 24 (66 percent) matches closely the amount of reaction inferred from the one-dimensional analysis (62 percent) shown in figure 13.

The center-line level of fuel concentration measured for the perpendicular injection strut ($\alpha \approx 0.027$) is of the same order as the maximum level of concentration ($\alpha \approx 0.025$) found for similar injection conditions and at the same axial location in the nonreactive mixing tests reported in reference 10. More detailed comparison with reference 10 is not feasible since only a small amount of composition data has been taken here for perpendicular injection, and no theory is available to predict the perpendicular injection flow field.

CONCLUDING REMARKS

Exploratory tests of two simple fuel injection struts for supersonic combustion, one with parallel injectors and one with perpendicular injectors, have been described. Results with each strut in a free-jet, short-duct, and long-duct test configuration at conditions simulating Mach 7 flight were presented and analyzed. Generally speaking, the mechanical and thermal designs of the struts were adequate for the severe test environment after material upstream of the leading-edge cooling tube was removed. The mixing-reacting flow fields produced by the injectors appear to be steady, and flame photographs have an orderly appearance with regularly spaced emission zones corresponding to the location of individual injection ports. No strong shock waves generated by combustion were observed in photographs of the flow fields. Good agreement was obtained between measured static-pressure distributions in the duct downstream of the strut injectors and distributions calculated with a one-dimensional analysis. The amount of reaction with length for the calculations was obtained from mixing calculations and correlations of nonreactive mixing data. For both parallel and perpendicular injection, this approach proved to be adequate to model the overall behavior of the strut injector flow fields including duct heat load, although heat load was underestimated when large separated regions occurred near the injection location.

Exit pitot-probe measurements generally agreed with the one-dimensional calculations when the duct exit shock structure (due to overexpansion) did not interfere with the measurements. The smoothness or lack of smoothness of pitot-pressure data was found to correlate qualitatively with the uniformity of the fuel distribution at the duct exit as determined from gas sample measurements. For the parallel injection strut, good agreement was obtained between the shape of the injected fuel distribution inferred from gas sample measurements and the distribution calculated with a multiple-jet mixing theory. For the multiple-jet calculation, approximately 25 percent increase in the single-jet value of eddy viscosity was required to obtain agreement with the data at the proper axial location. The overall fraction of injected fuel reacted in the multiple-jet calculation also closely matched the amount of fuel reacted in the one-dimensional calculation which gave good agreement with duct static-pressure data. Similarly, gas sample measurements

with the perpendicular injection strut gave results consistent with the amount of fuel reacted in the one-dimensional calculation.

Langley Research Center,
National Aeronautics and Space Administration,
Hampton, Va., January 21, 1974.

REFERENCES

1. Henry, J. R.; and McLellan, C. H.: Air-Breathing Launch Vehicle for Earth-Oribt Shuttle – New Technology and Development Approach. J. Aircraft, vol. 8, no. 5, May 1971, pp. 381-387.

2. Becker, John V.: New Approaches to Hypersonic Aircraft. Paper presented at Seventh Congress of International Council of Aeronautical Sciences (Rome, Italy), Sept. 1970.

3. Henry, John R.; and Beach, H. Lee: Hypersonic Air-Breathing Propulsion Systems. Vehicle Technology for Civil Aviation – The Seventies and Beyond, NASA SP-292, 1971, pp. 157-177.

4. Metzler, A. J.; and Mertz, T. W.: Large Scale Supersonic Combustor Testing at Conditions Simulating Mach 8 Flight. AIAA Paper No. 70-715, June 1970.

5. Henry, John R.; and Anderson, Griffin Y.: Design Considerations for the Airframe-Integrated Scramjet. NASA TM X-2895, 1973.

6. Beach, H. L., Jr.: Supersonic Mixing and Combustion of a Hydrogen Jet in a Coaxial High-Temperature Test Gas. AIAA Paper No. 72-1179, Nov.-Dec. 1972.

7. Hopf, H.; and Fortune, O.: Diffusion Controlled Combustion for Scramjet Application. Pt. II – Programmer's Manual. Tech. Rep. 569 (Contract NAS 1-5117), Marquardt Corp., Dec. 1965. (Available as NASA CR-66717.)

8. Eggers, James M.: Turbulent Mixing of Coaxial Compressible Hydrogen-Air Jets. NASA TN D-6487, 1971.

9. Alzner, Edgar: Three Dimensional Mixing of Jets. ATL TR 150 (Contract NAS 1-4560), Advanced Technologies Lab., Inc. July 1970. (Available as NASA CR-111782.)

10. Rogers, R. Clayton: Mixing of Hydrogen Injected From Multiple Injectors Normal to a Supersonic Airstream. NASA TN D-6476, 1971.

11. Russin, William Roger: Performance of a Hydrogen Burner To Simulate Air Entering Scramjet Combustors. NASA TN D-7567, 1974.

12. Rogers, R. C.; and Eggers, J. M.: Supersonic Combustion of Hydrogen Injected Perpendicular to a Ducted Vitiated Airstream. AIAA Paper No. 73-1322, Nov. 1973.

13. Billig, F. S.; and Dugger, G. L.: The Interaction of Shock Waves and Heat Addition in the Design of Supersonic Combustors. Twelfth Symposium (International) on Combustion, Combust. Inst., c.1969, pp. 1125-1139.

14. Pinckney, S. Z.: Method For Predicting Compressible Turbulent Boundary Layers in Adverse Pressure Gradients. NASA TM X-2302, 1971.

INPUT

1. Geometry

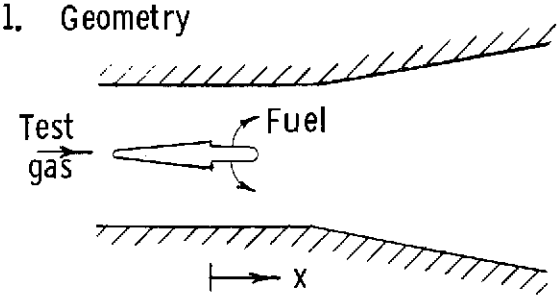

2. Entrance conditions

3. Fuel injection distribution

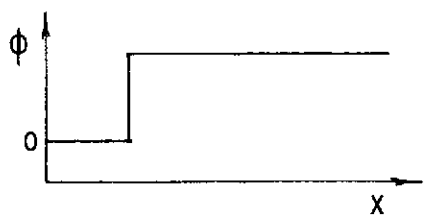

4. Fuel reaction distribution

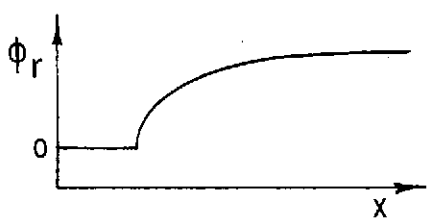

5. Wall friction coefficient and wall temperature

OUTPUT

1. Flow state

2. Wall heat flux

Figure 1.- Flow model for one-dimensional analysis.

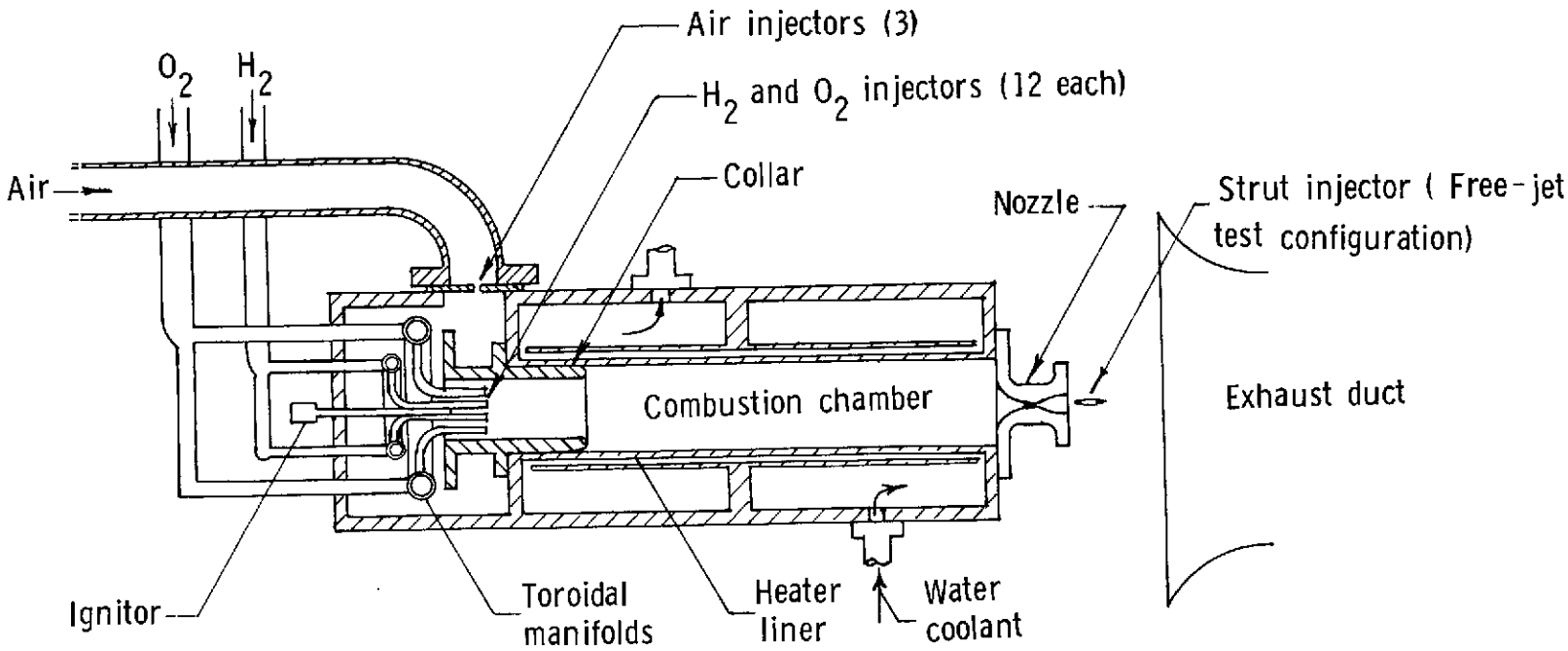

Figure 2.- Test gas supply burner.

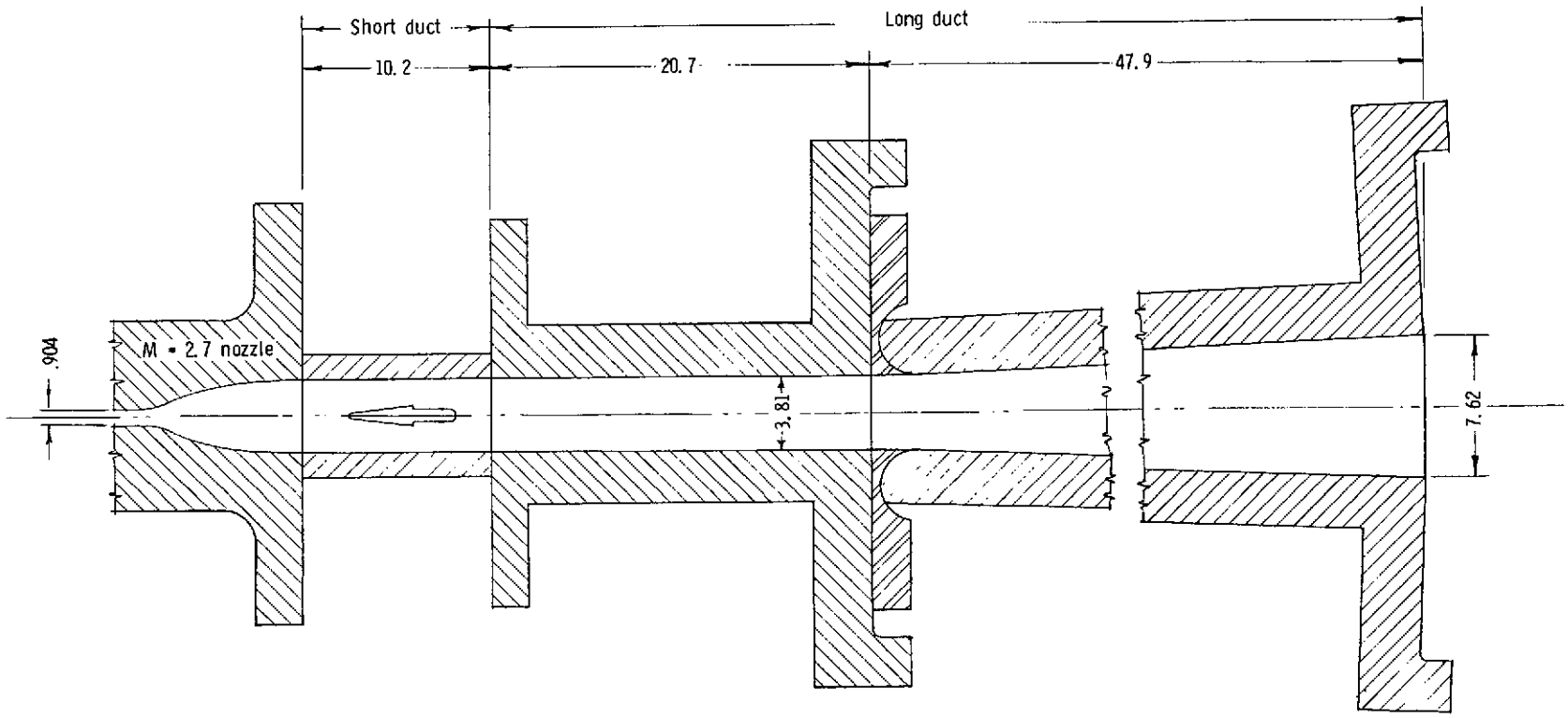

Figure 3.- Strut injector and two-dimensional combustion duct. Dimensions are in centimeters.

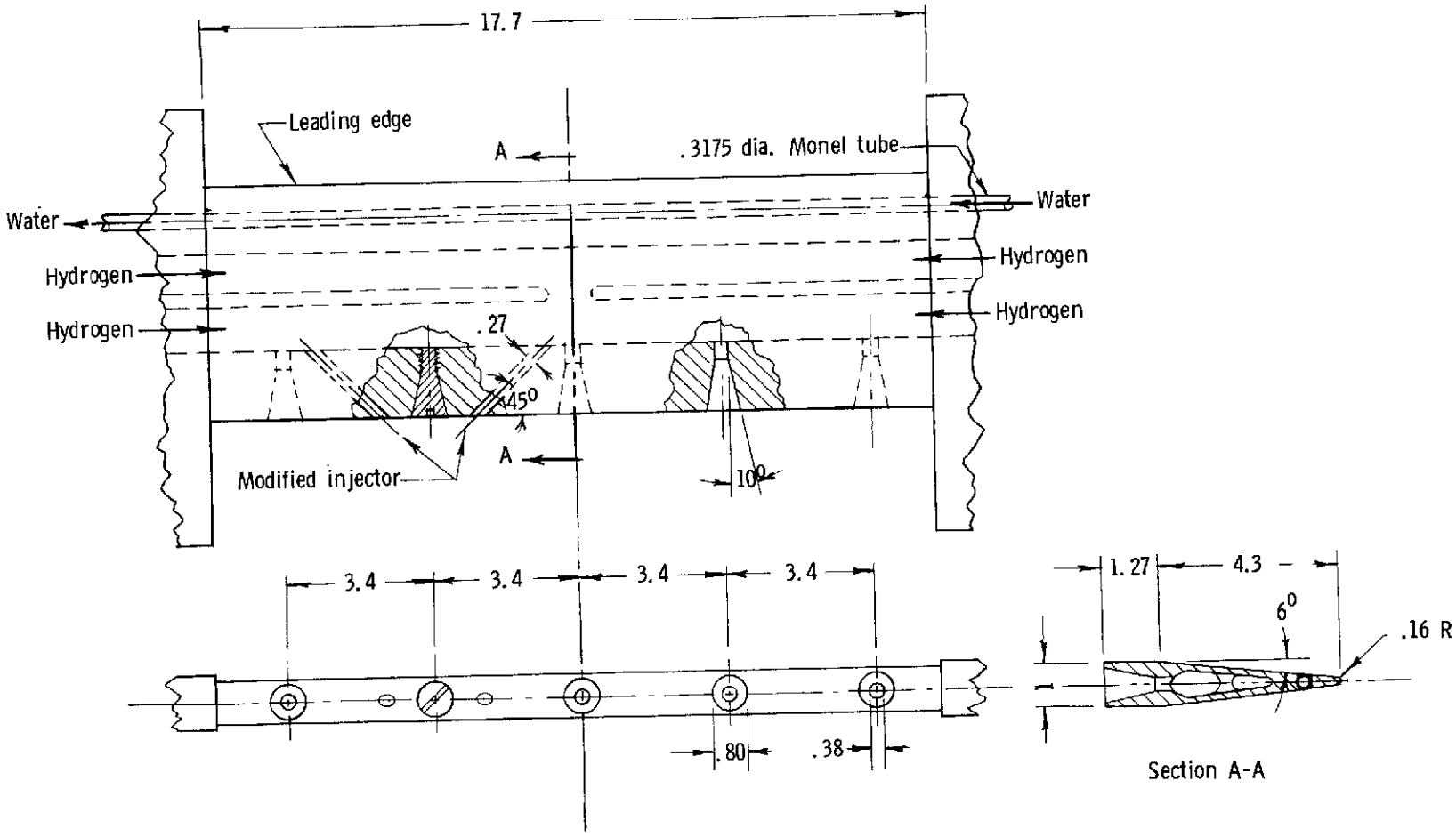

(a) Parallel injection strut.

Figure 4.- Strut injectors. (All dimensions are in cm.)

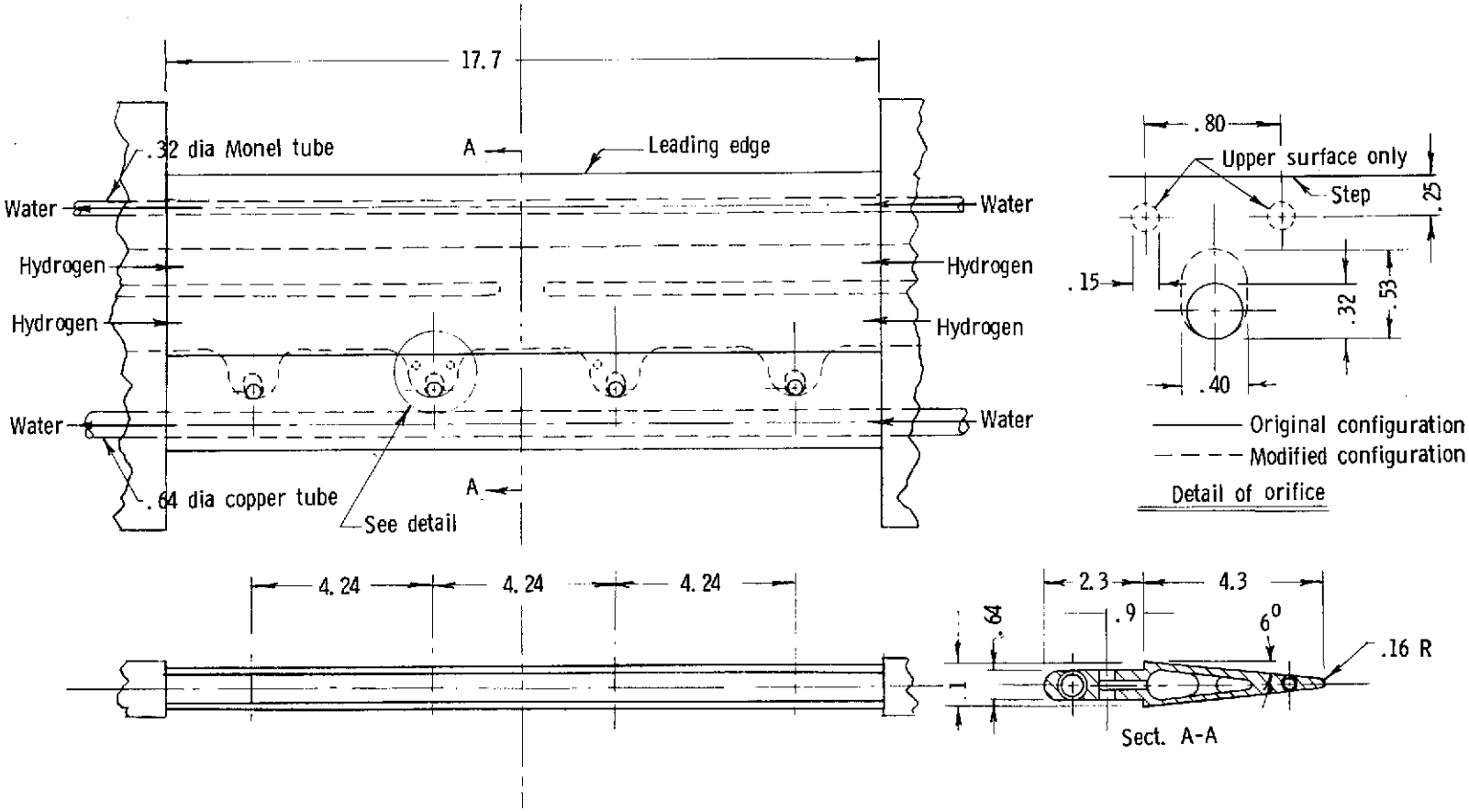

(b) Perpendicular injection strut.

Figure 4.- Concluded.

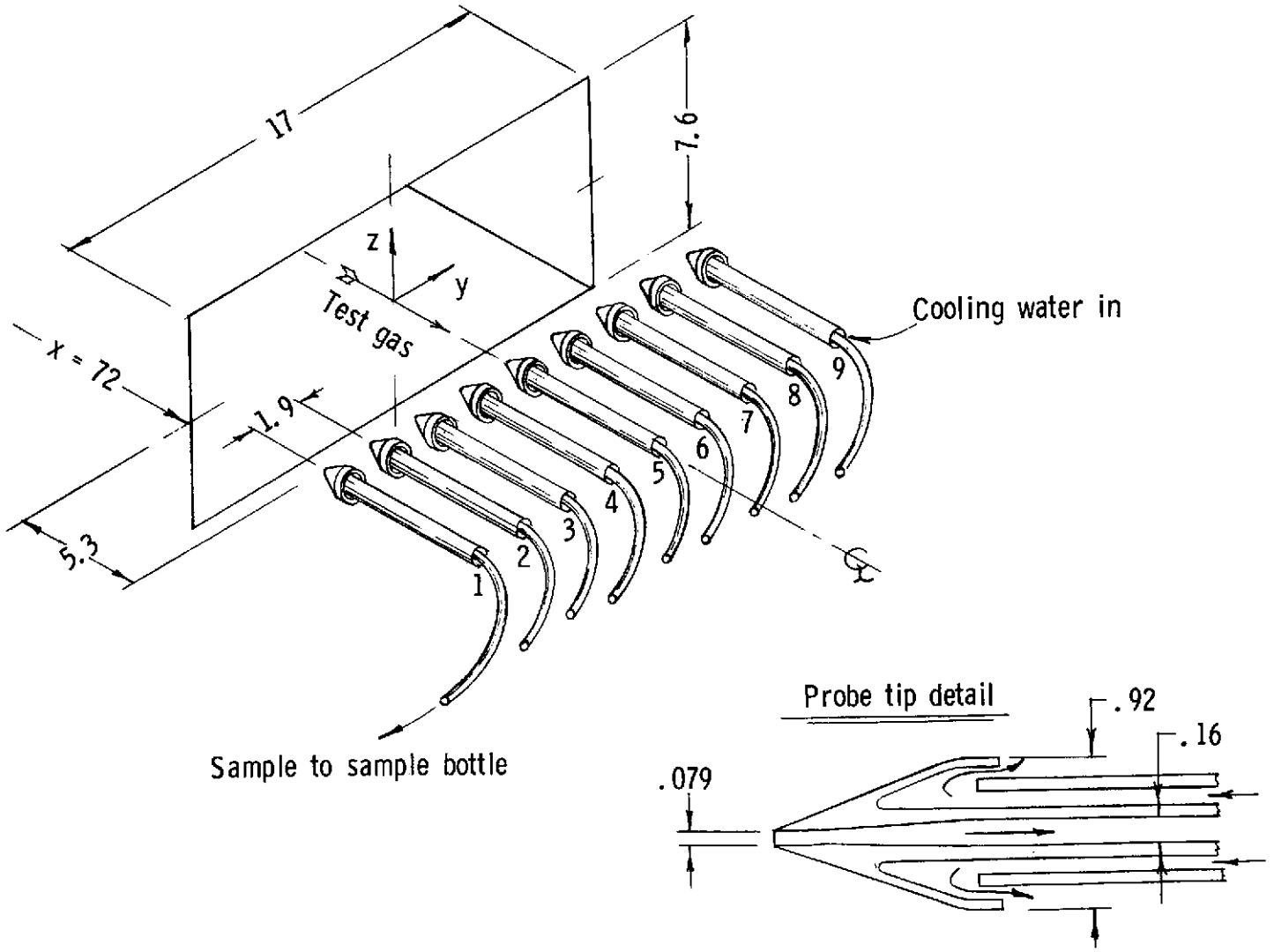

Figure 5.- Pitot and gas sample probe rake.

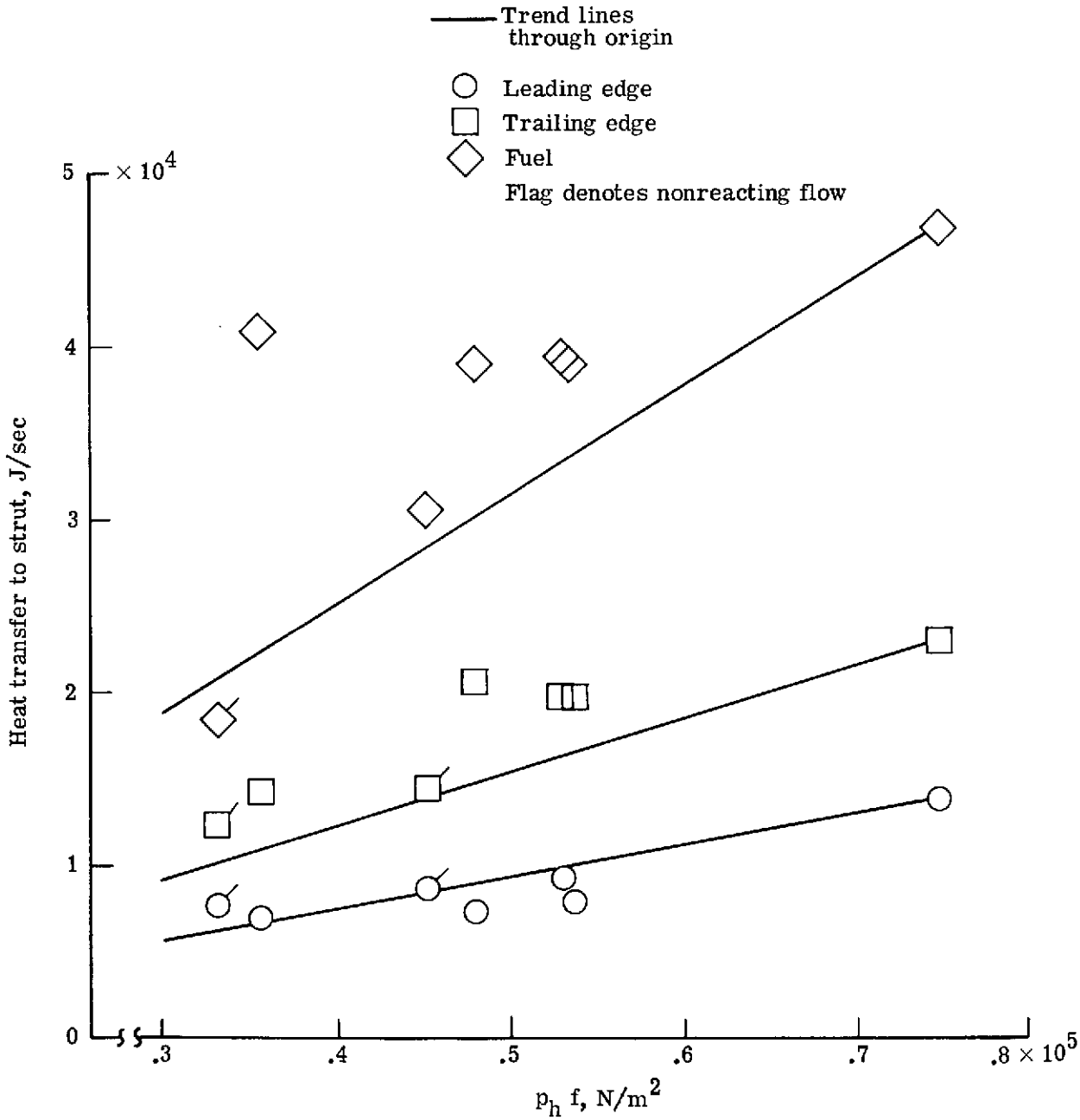

Figure 6.- Heat transfer to perpendicular injection strut. ϕ = 0.5 to 1.

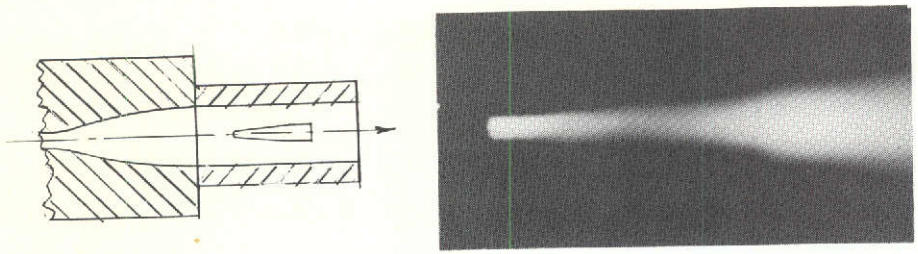

(a) Side view.

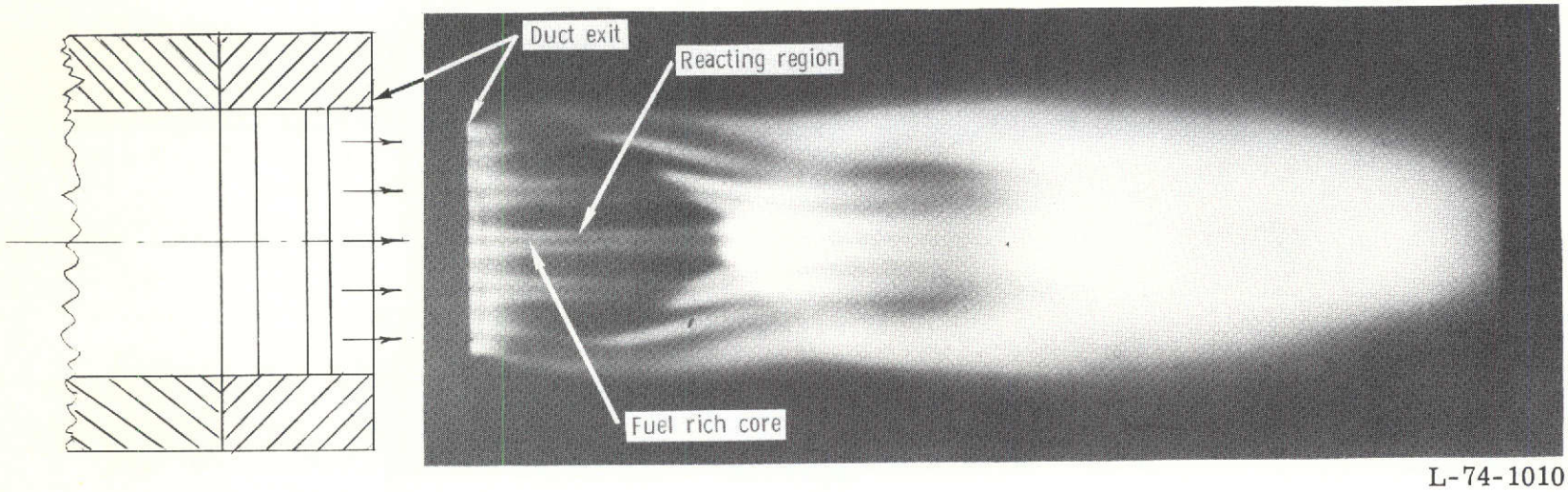

(b) Top view.

Figure 7.- Flame photograph of parallel injection strut in short duct.

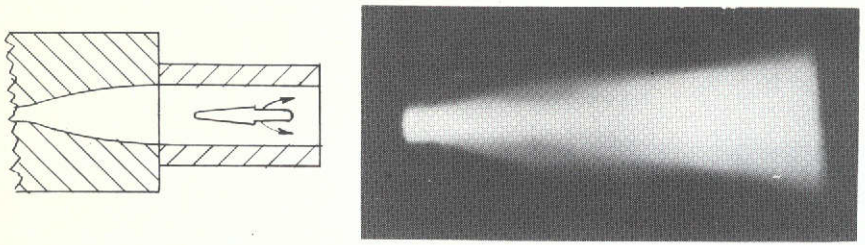

(a) Side view.

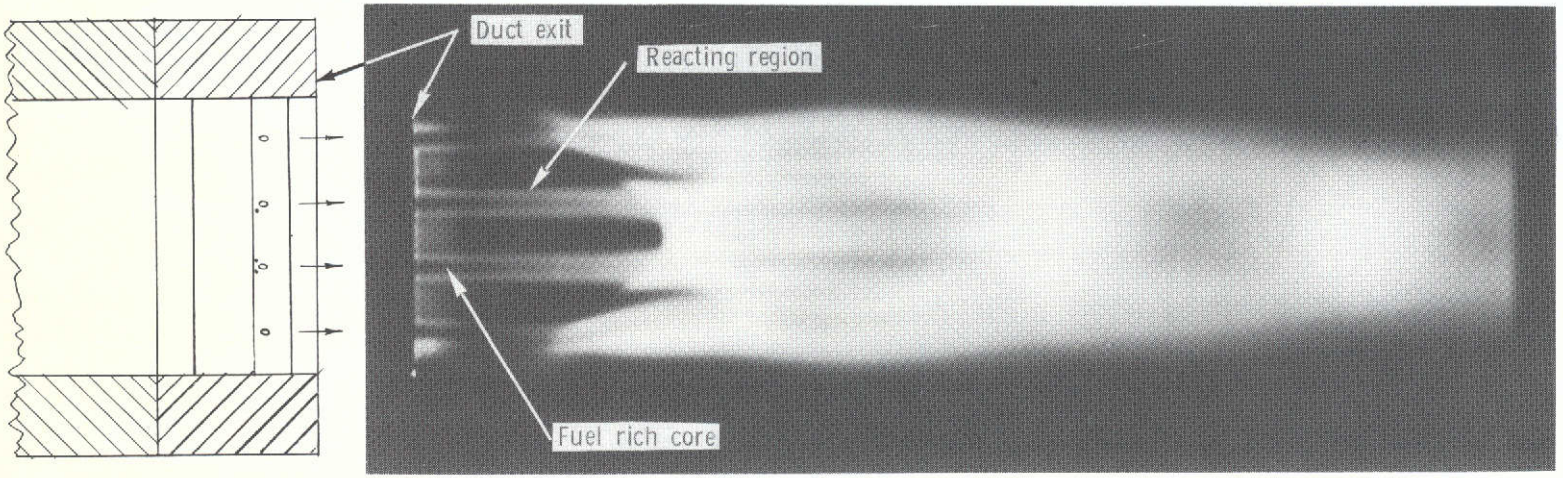

(b) Top view.

Figure 8.- Flame photograph of perpendicular injection strut in short duct.

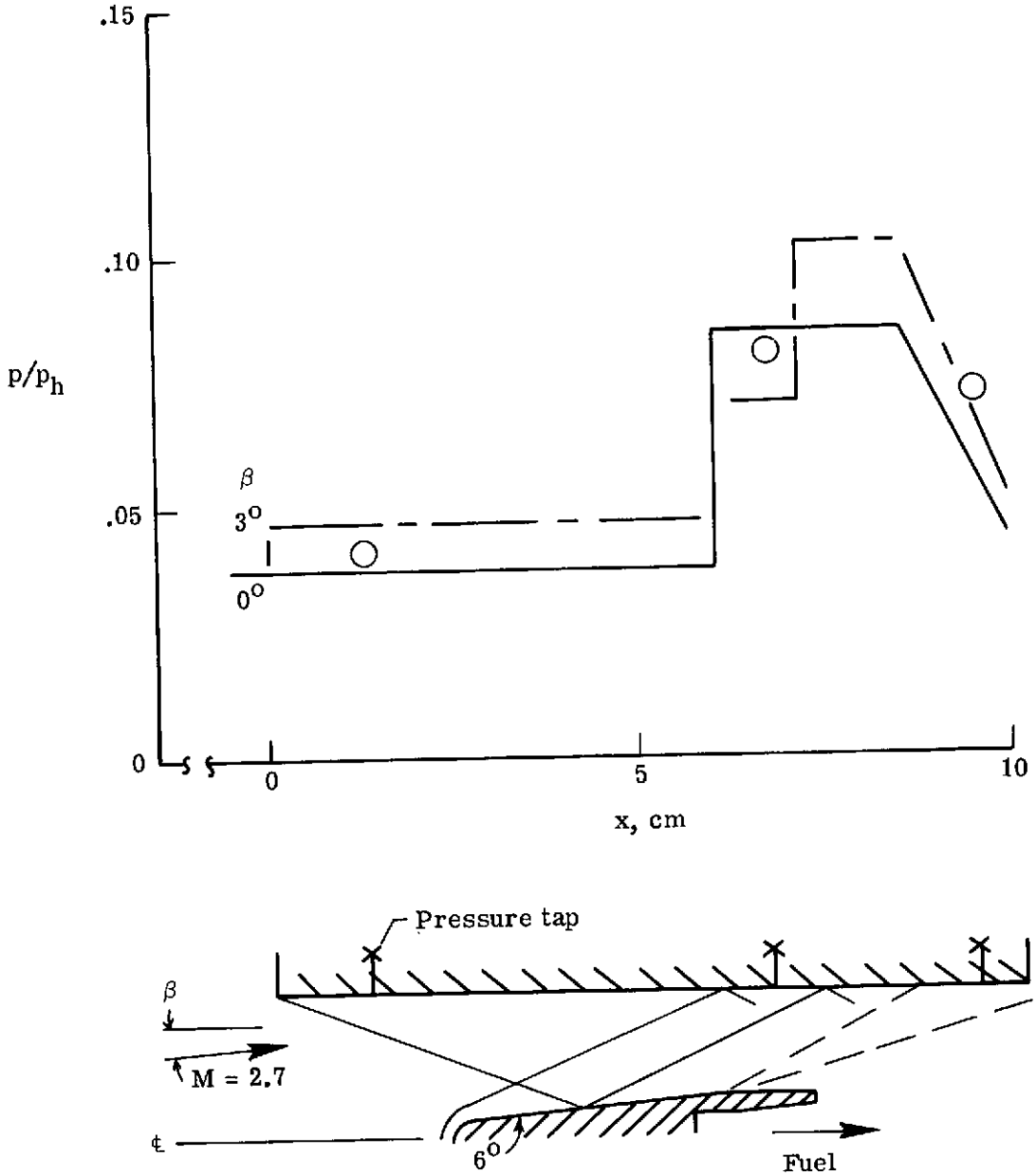

Figure 9.- Wall pressure in short duct with parallel injection strut. ϕ = 0.5 to 1.0.

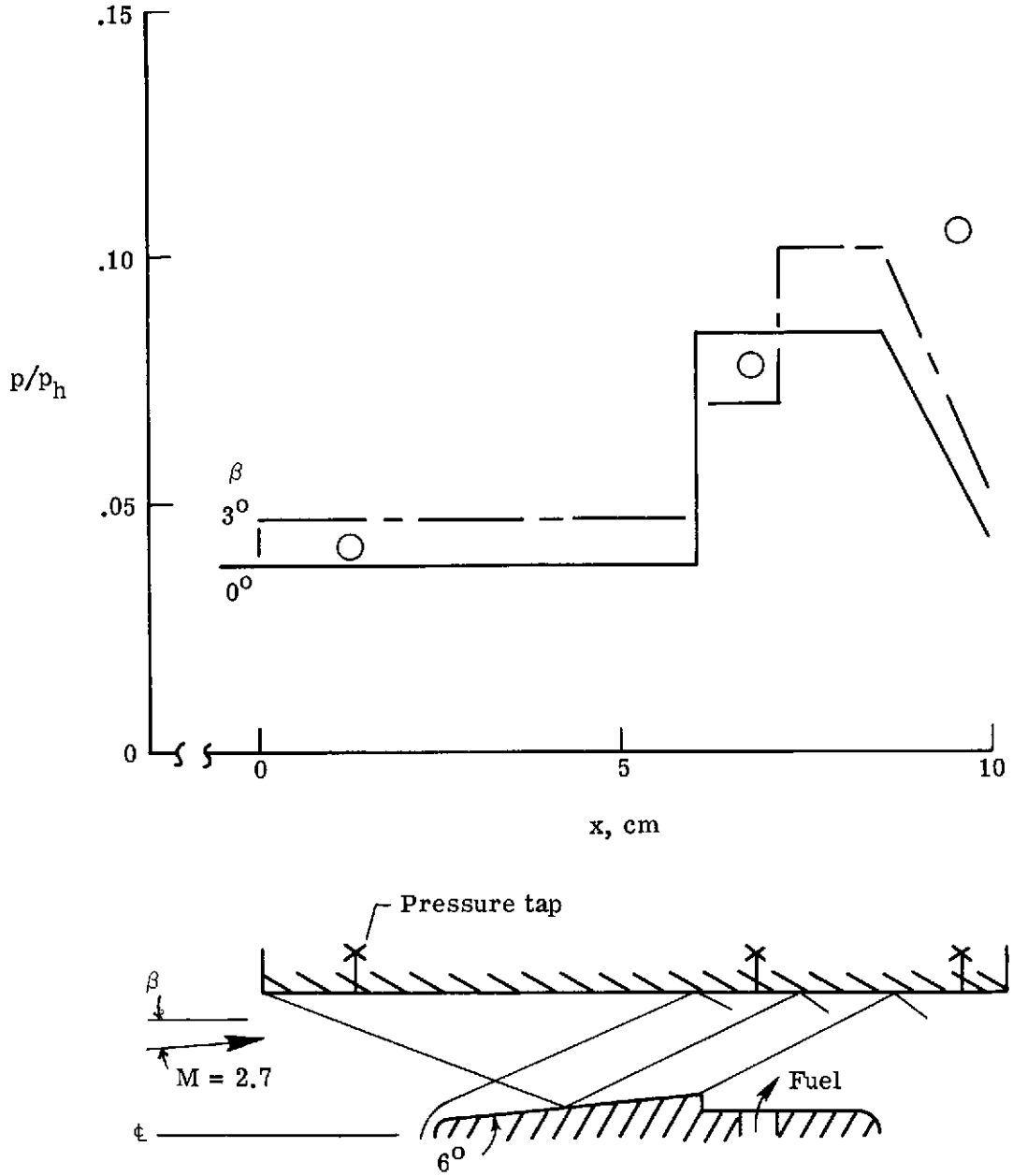

Figure 10.- Wall pressure in short duct with perpendicular injection strut. ϕ = 0.5 to 1.

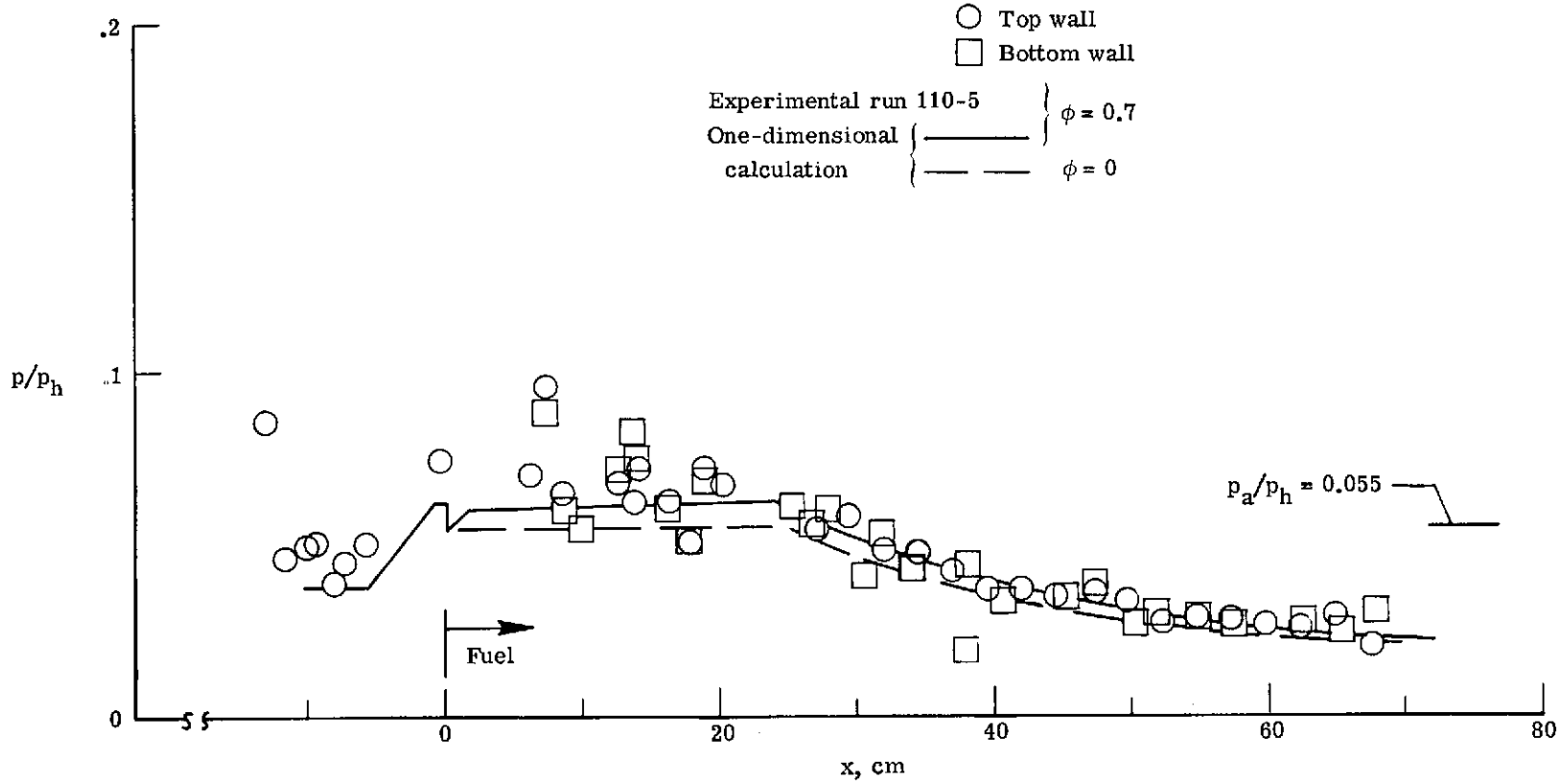

Figure 11.- Parallel injection strut without reaction. Run 110-5.

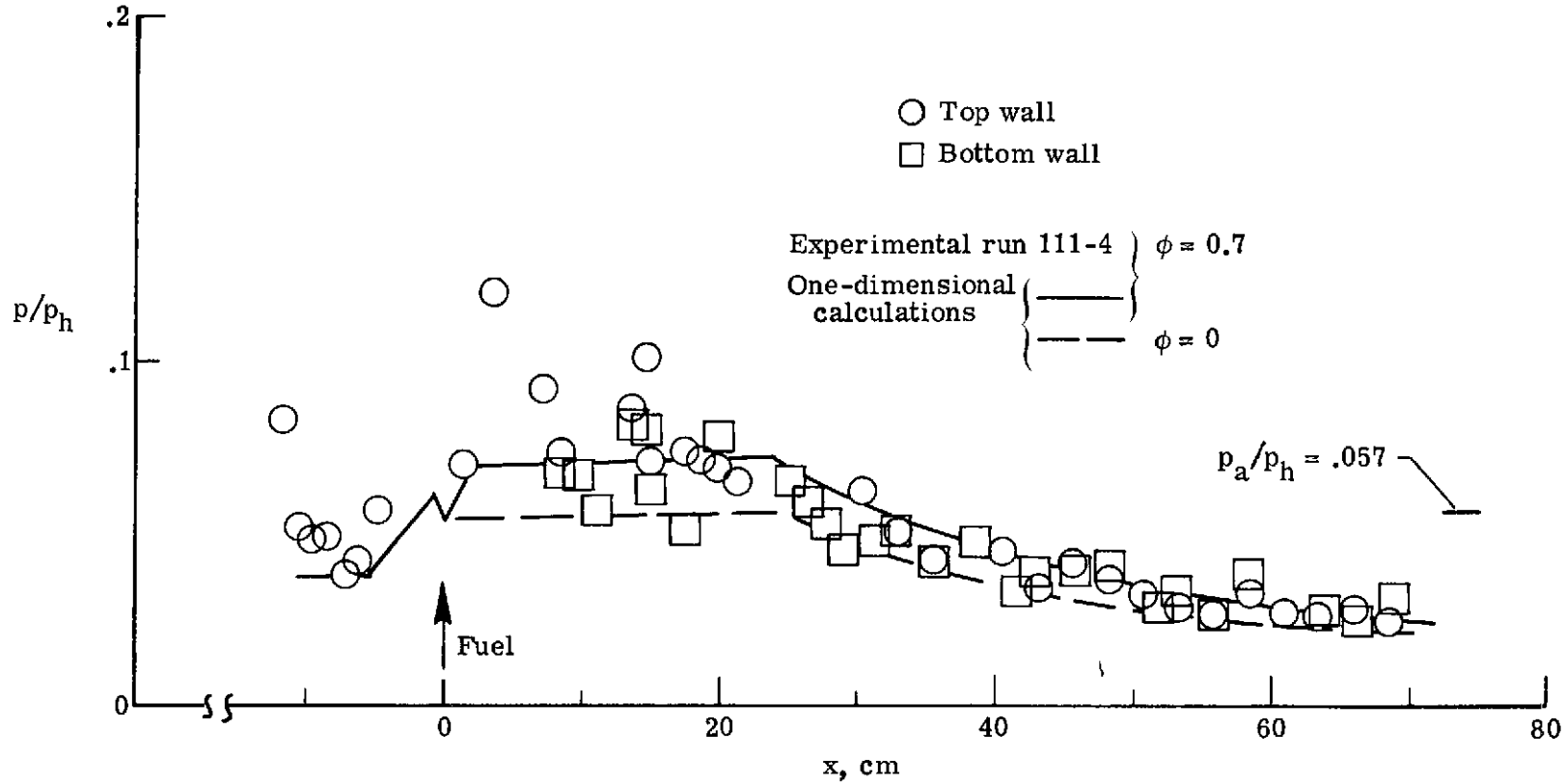

Figure 12.- Perpendicular injection strut without reaction. Run 111-4.

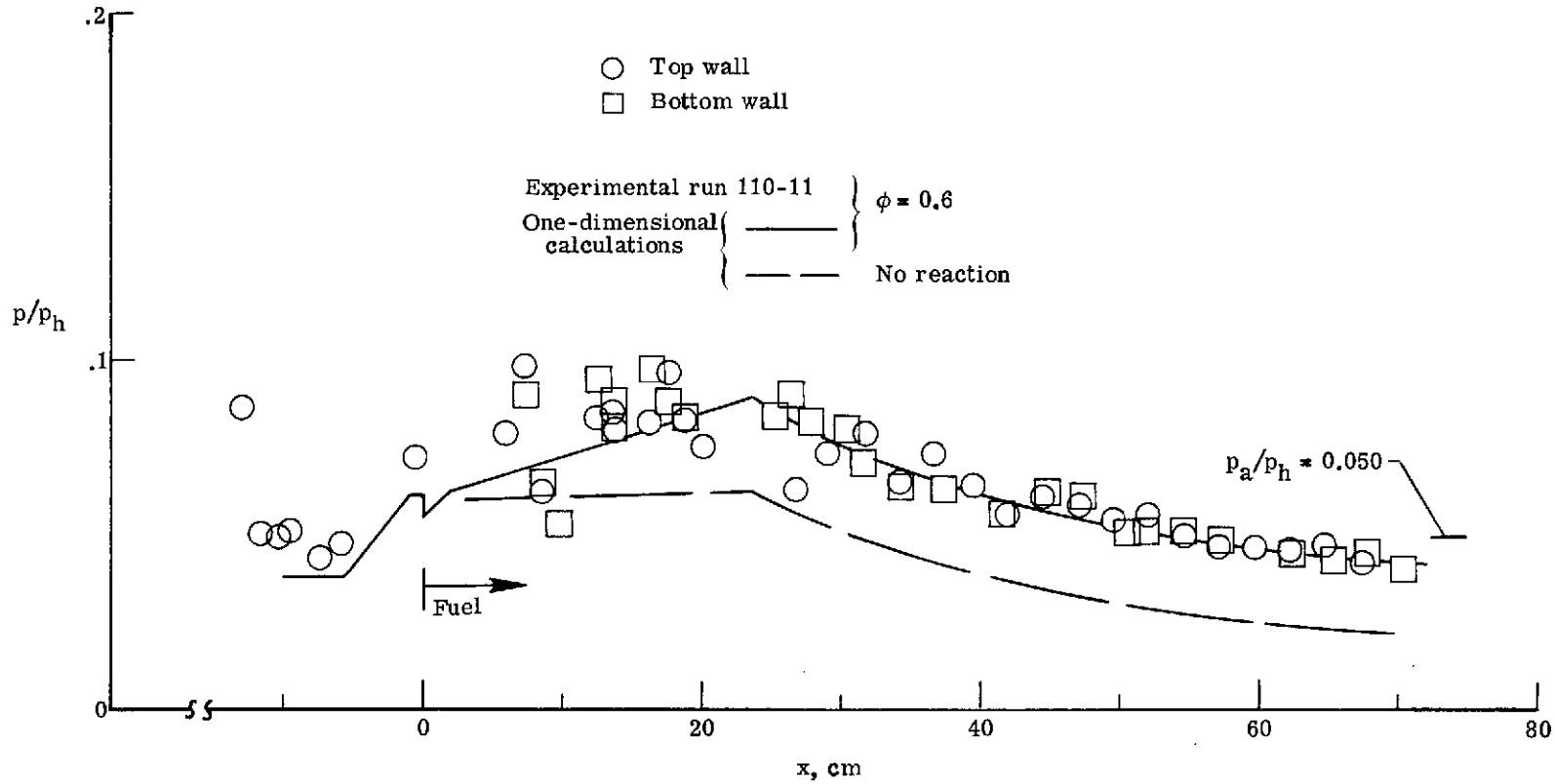

Figure 13.- Parallel injection strut with reaction. Run 110-11.

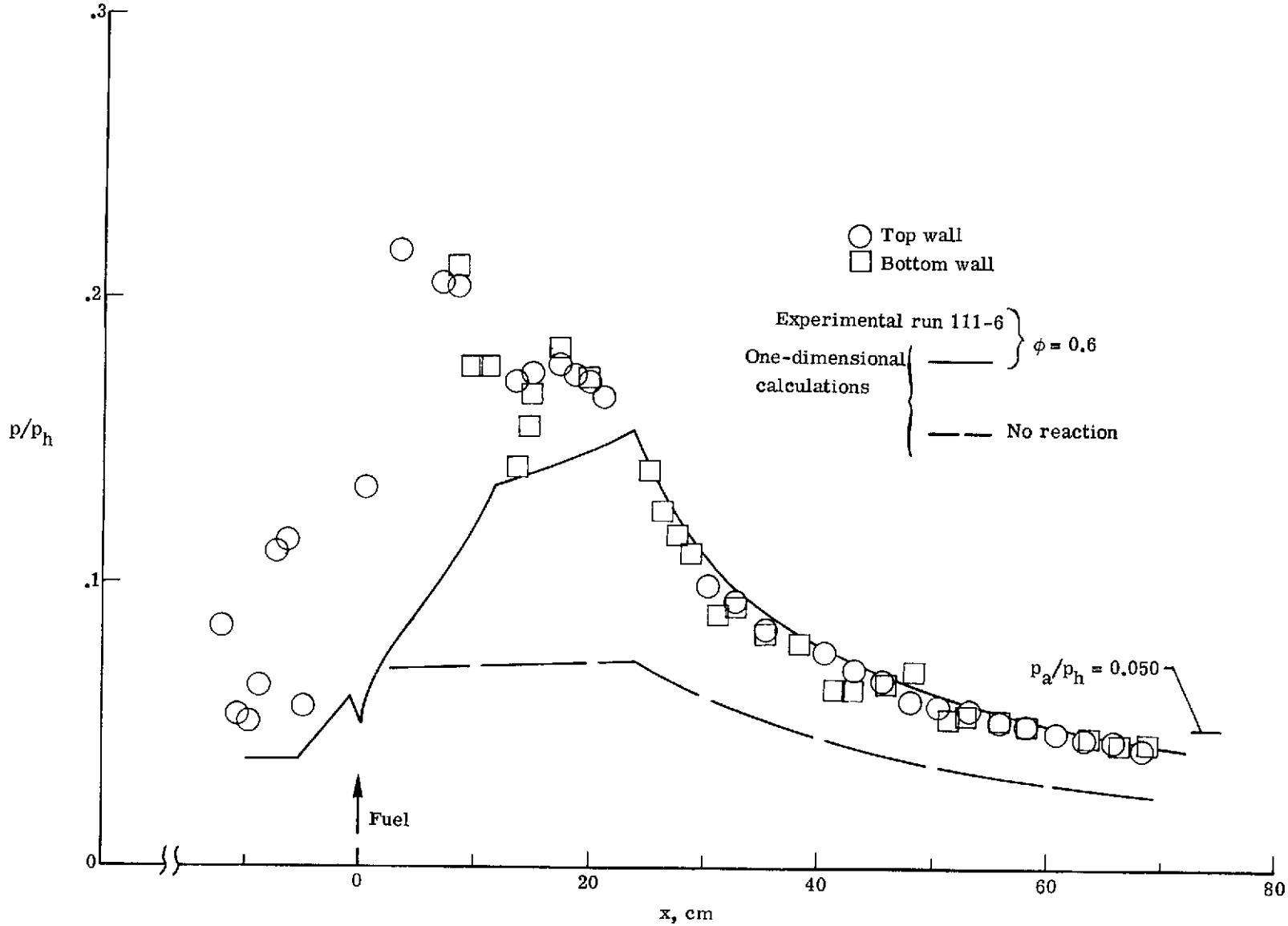

Figure 14.- Perpendicular injection strut with reaction. Run 111-6.

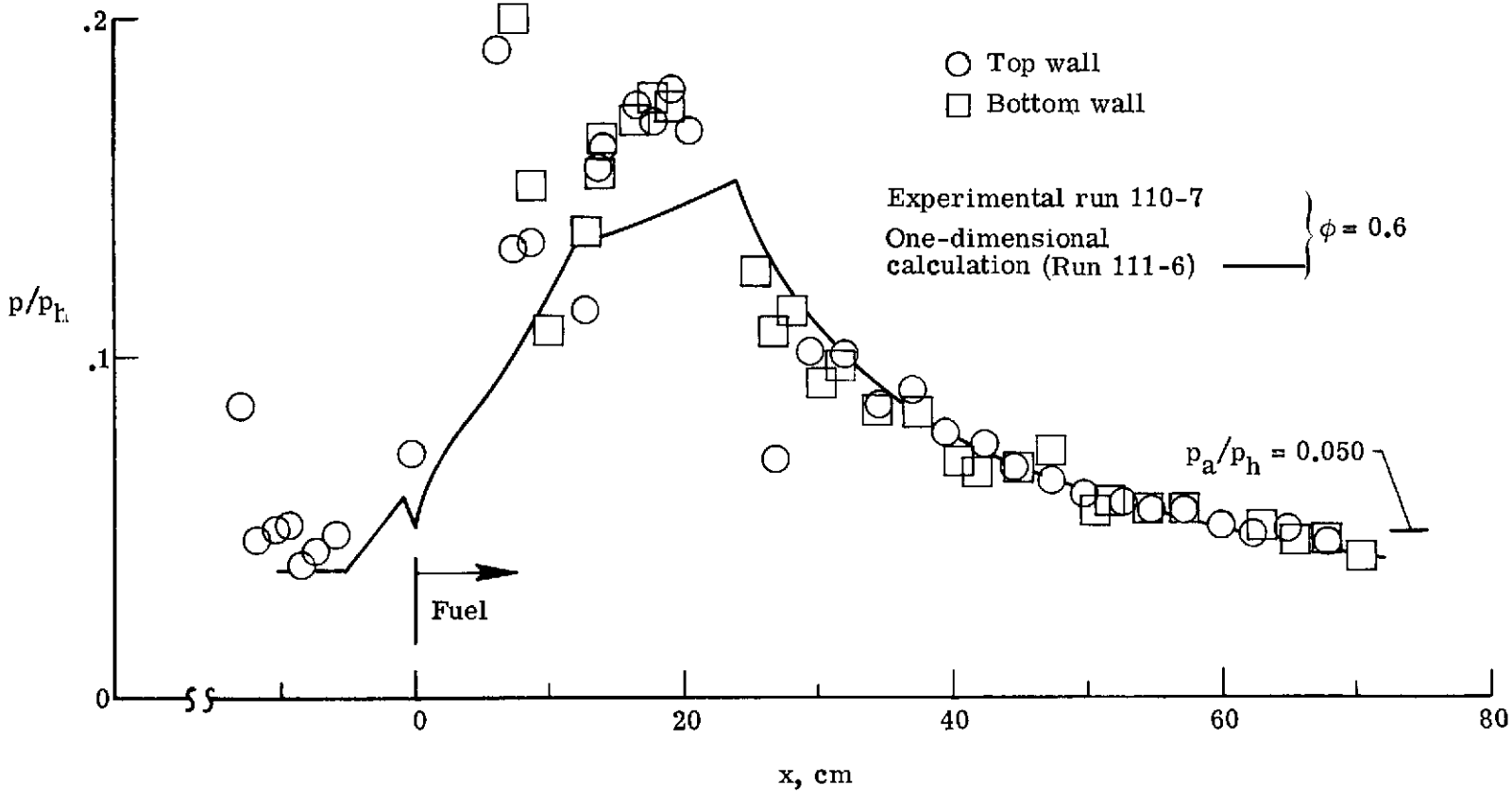

Figure 15.- Parallel injection strut with reaction. Run 110-7.

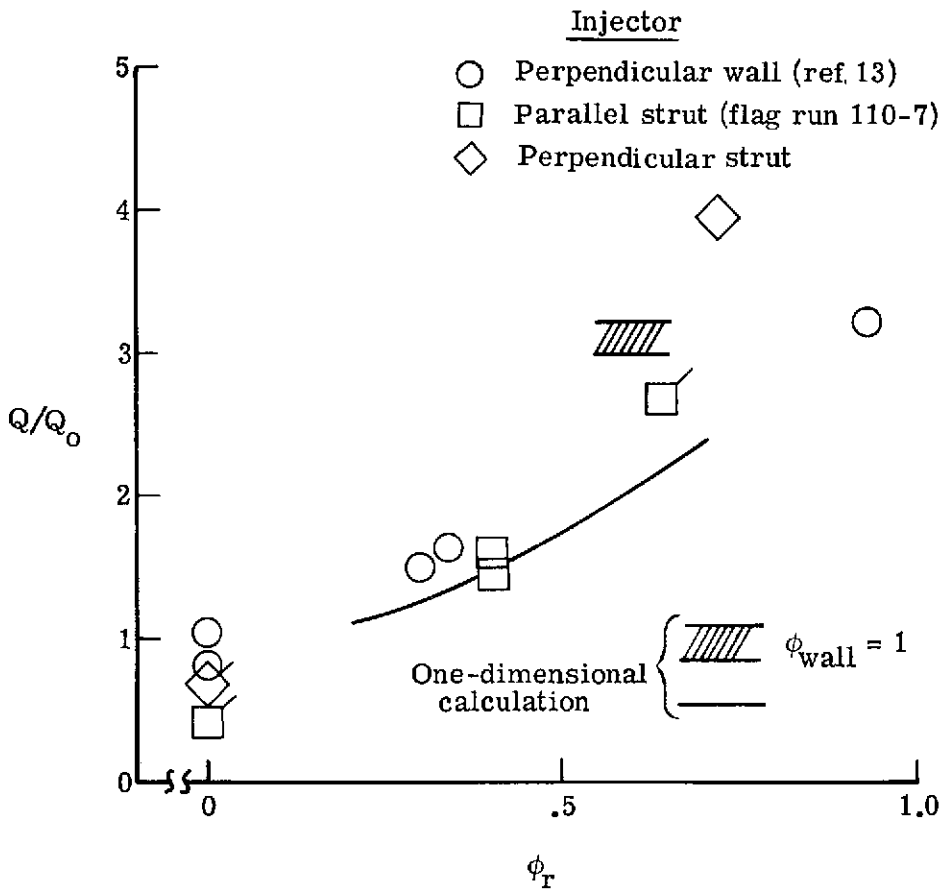

Figure 16.- Duct heat load.

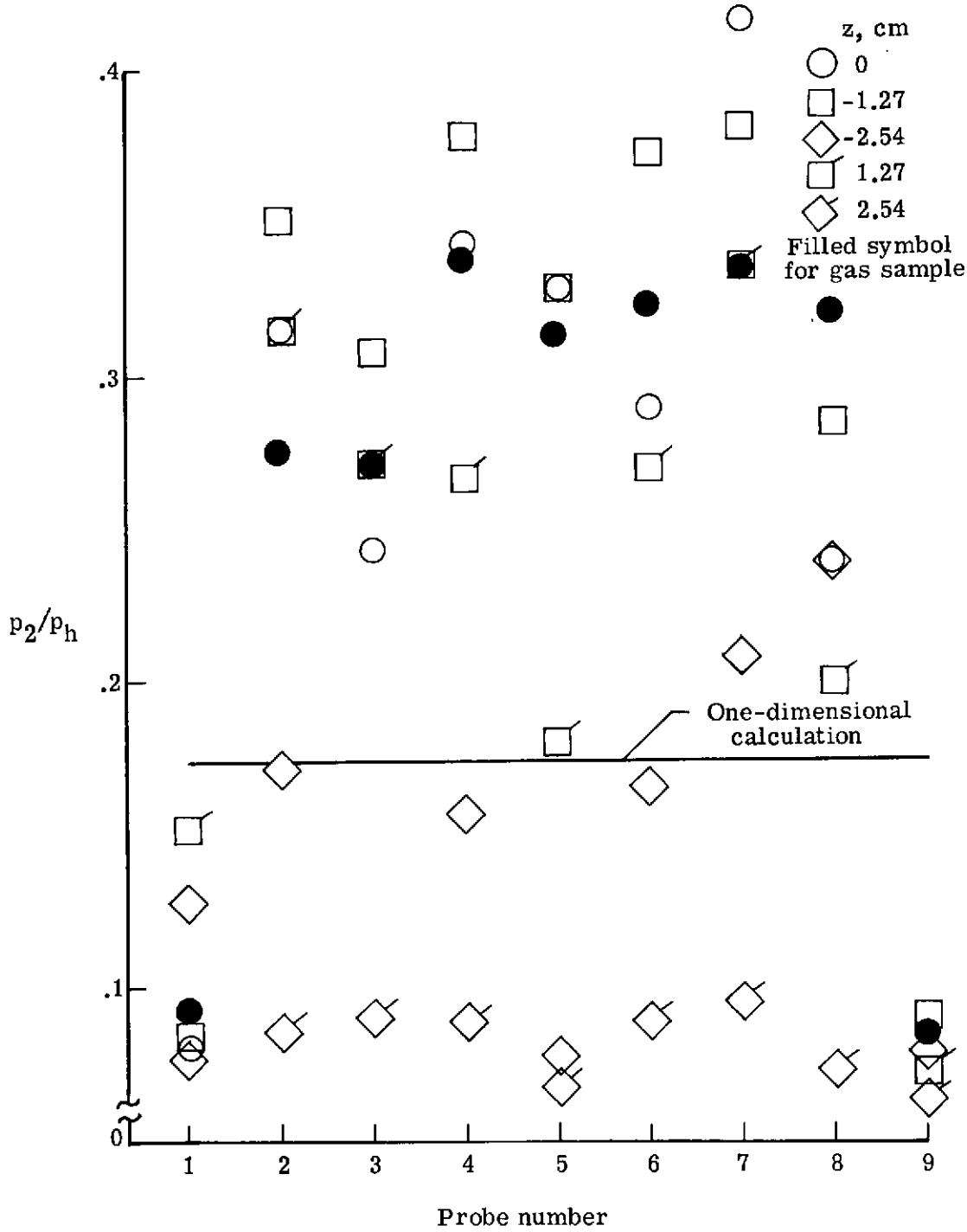

Figure 17.- Exit pitot pressure for parallel injection strut without reaction. Runs 110-5 and 110-6.

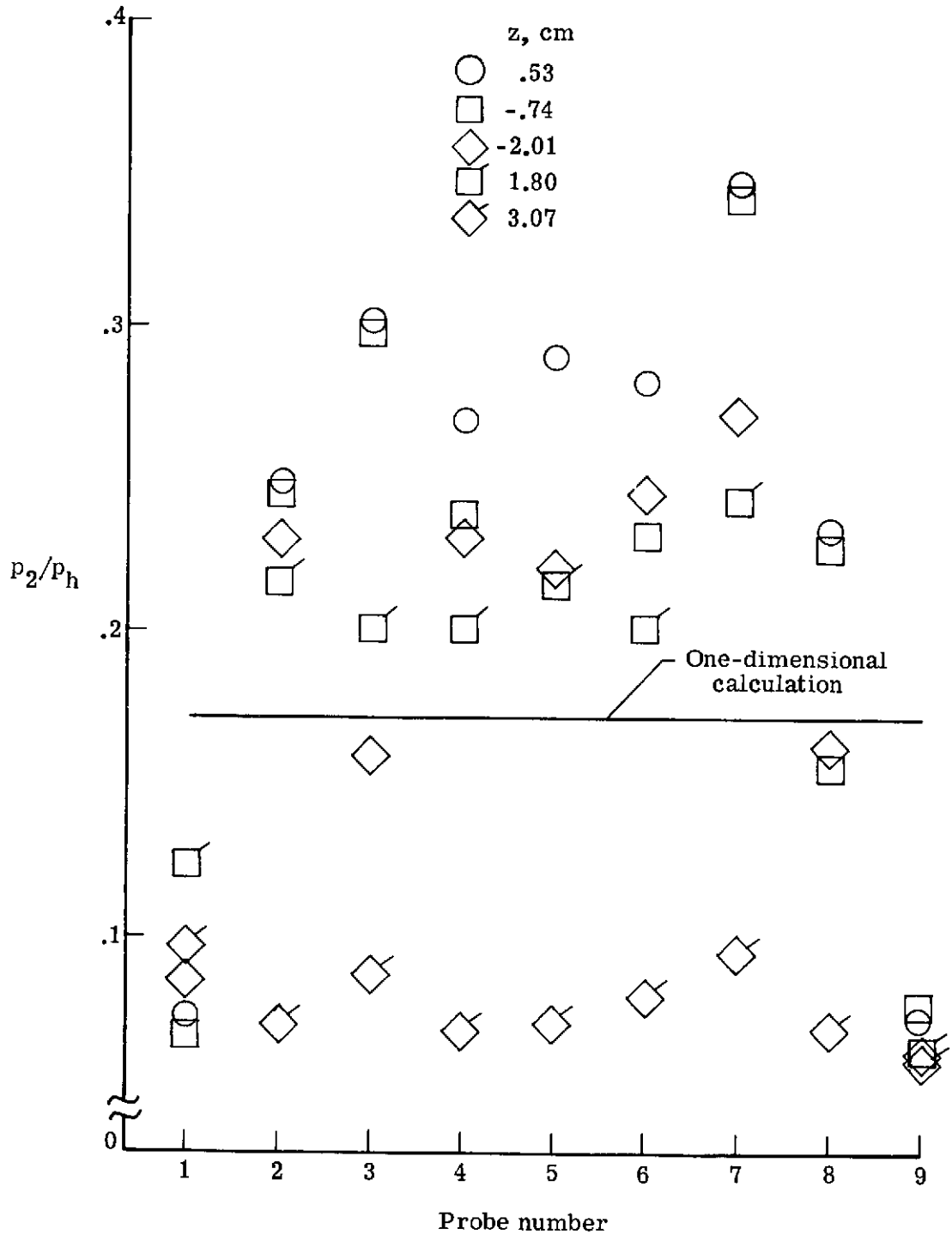

Figure 18.- Exit pitot pressure for perpendicular injection strut without reaction. Run 111-4.

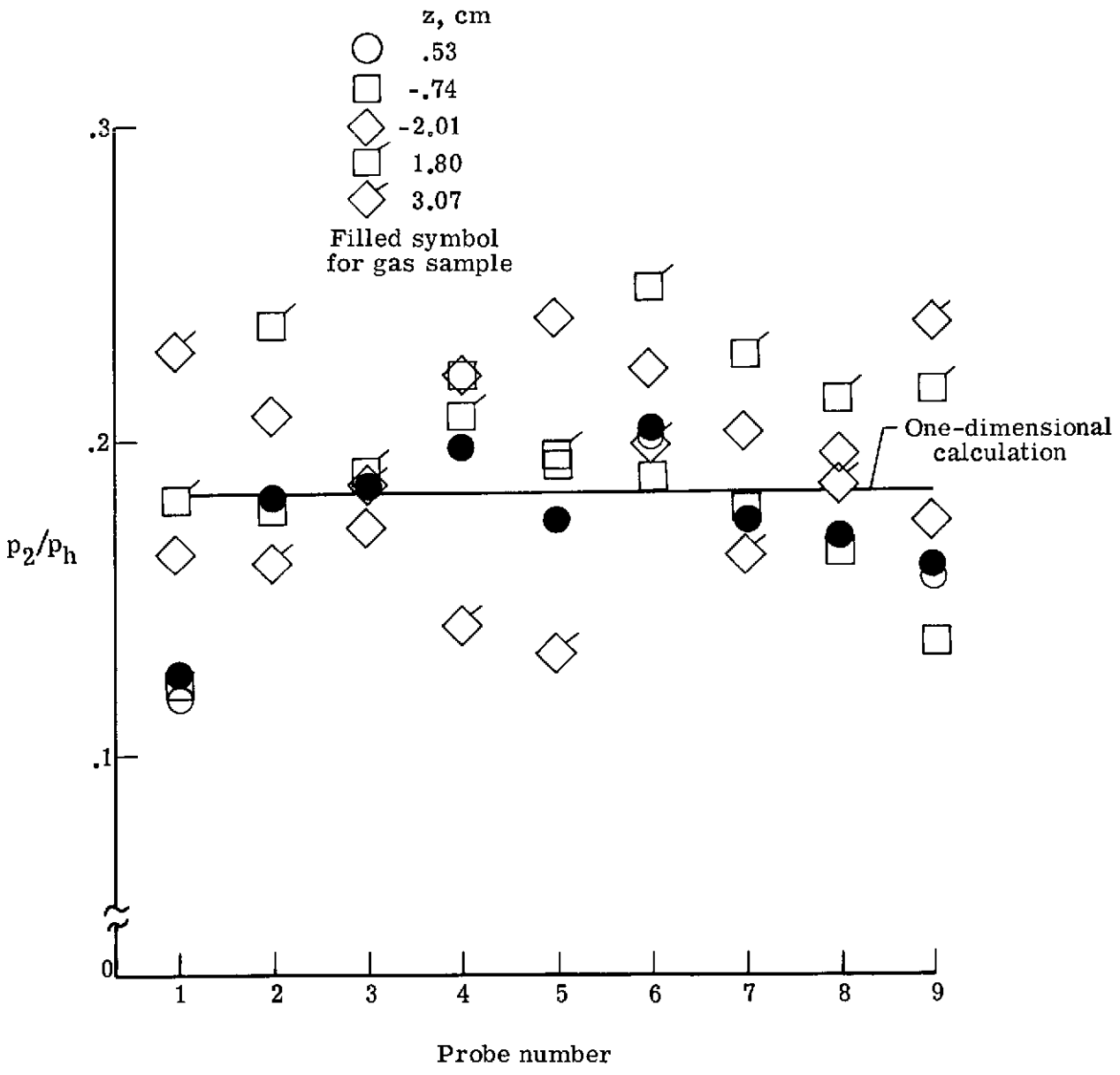

Figure 19.- Exit pitot pressure for parallel injection strut with reaction.

Runs 110-10 and 110-8.

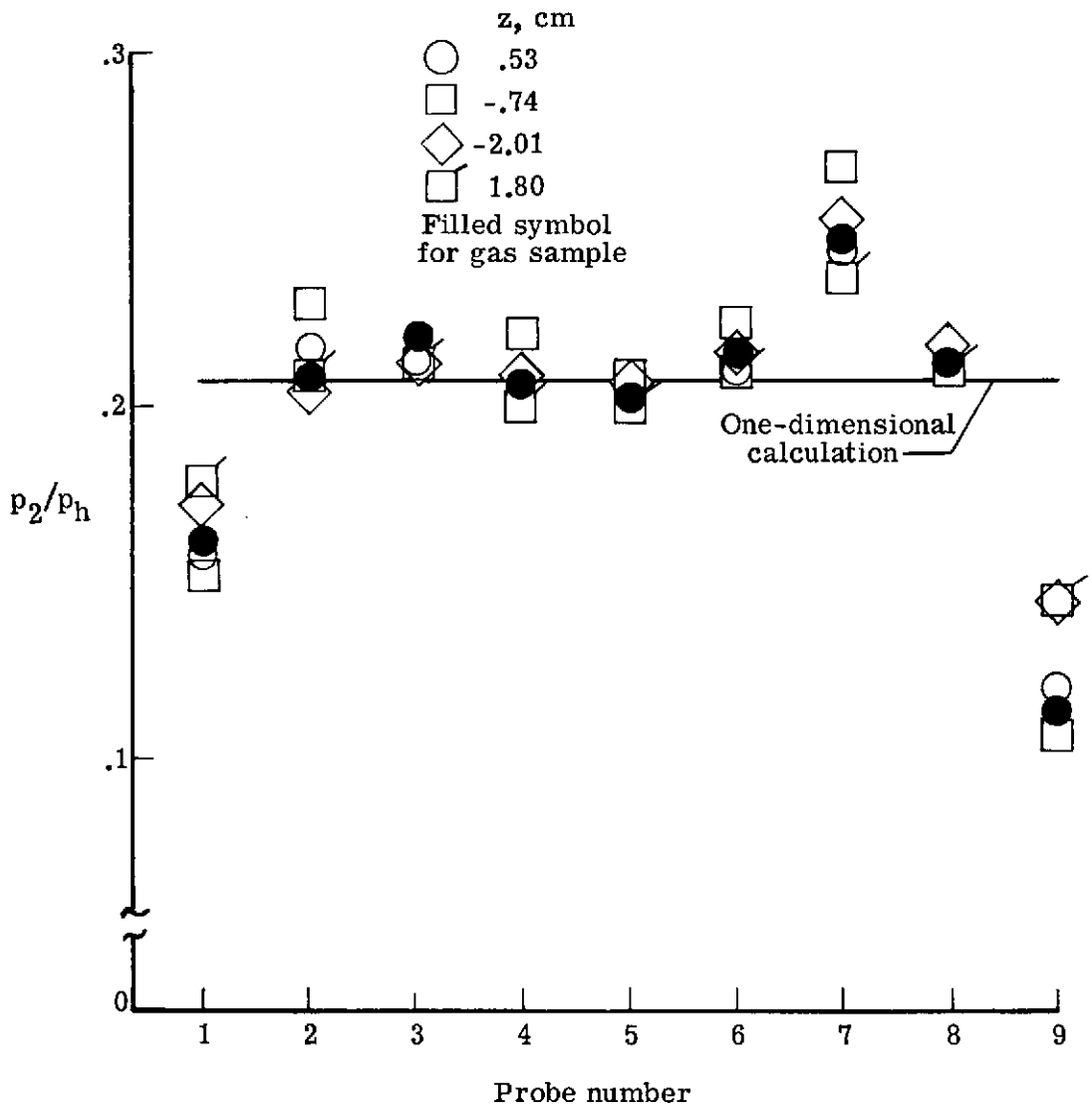

Figure 20.- Exit pitot pressure for perpendicular injection strut with reaction. Runs 111-5 and 111-6.

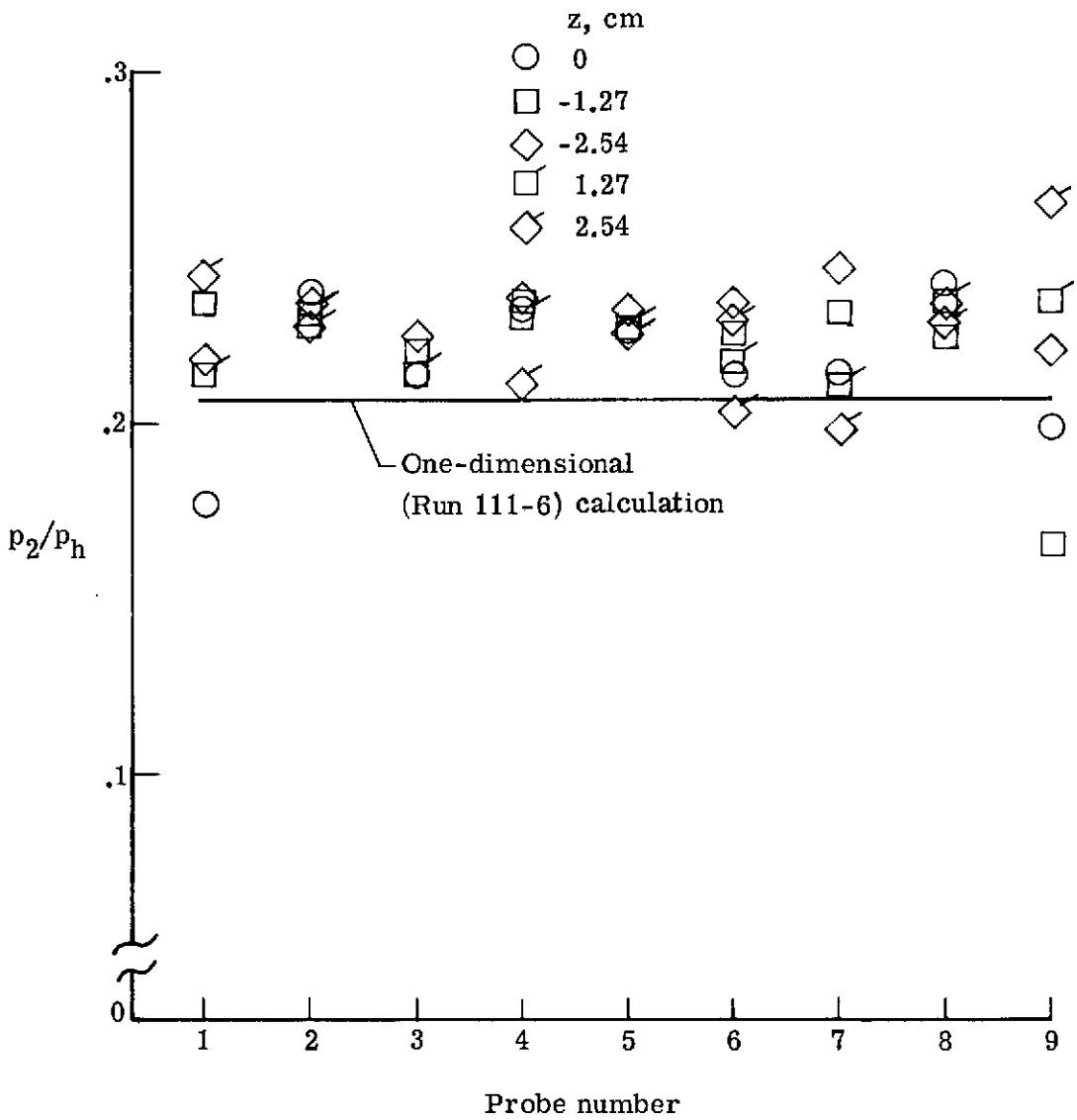

Figure 21.- Exit pitot pressure for parallel injection strut with reaction. Run 110-7.

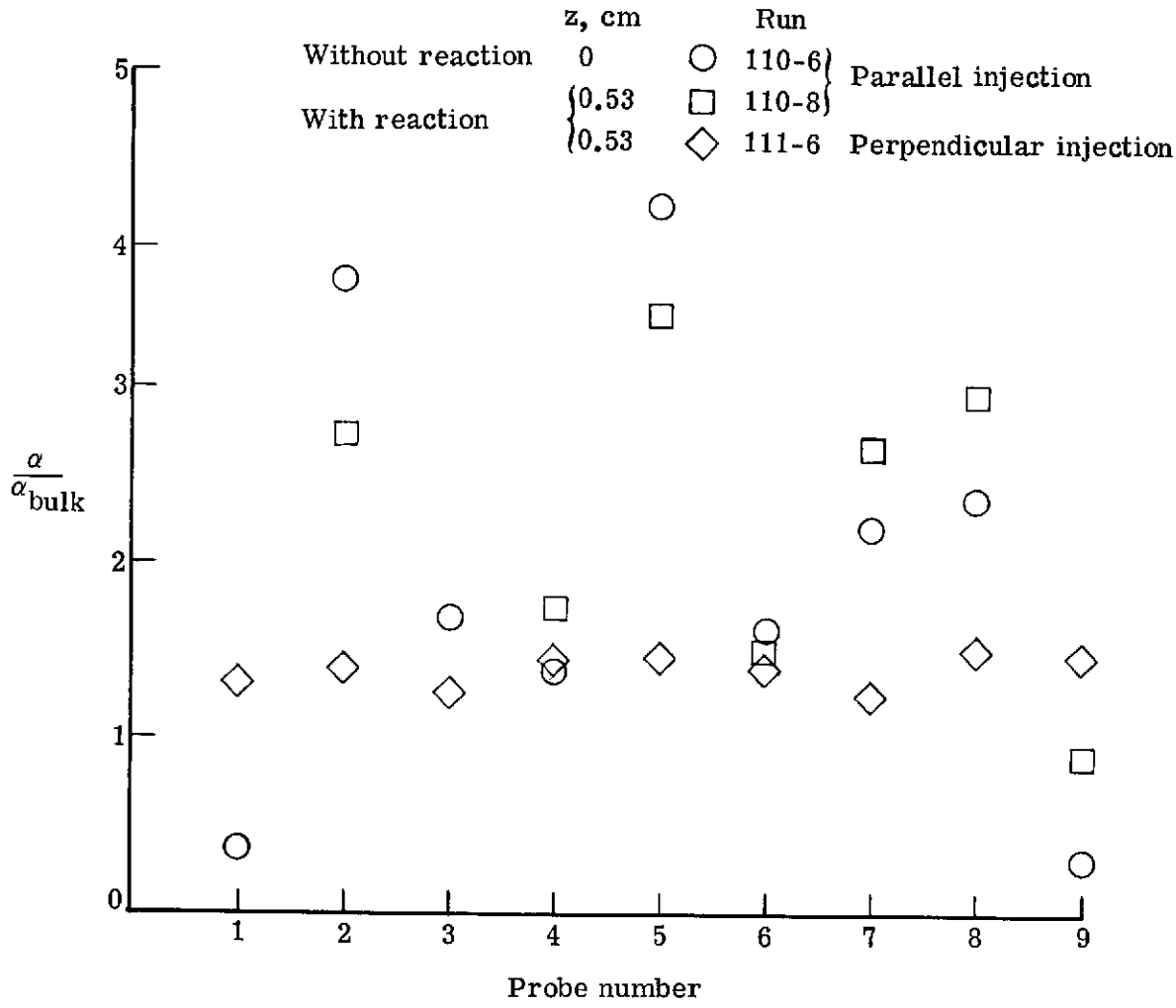

Figure 22.- Gas sample data.

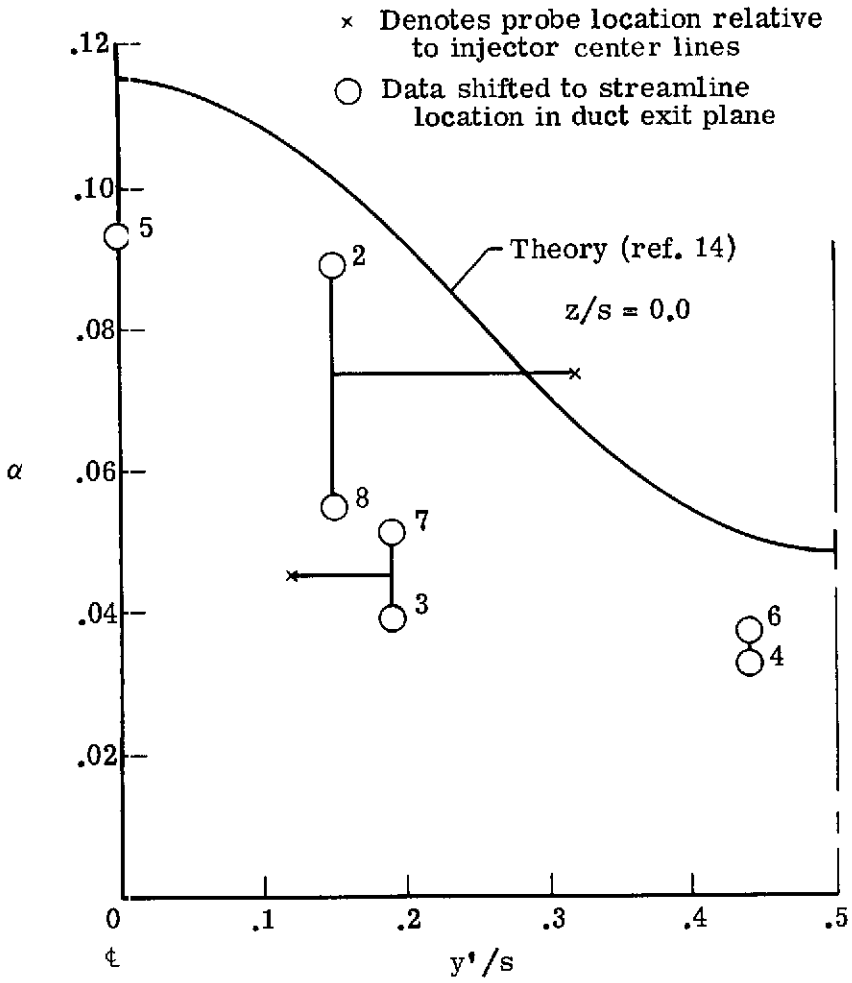

Figure 23.- Parallel injection strut fuel distribution without reaction compared with theory. Run 110-6.

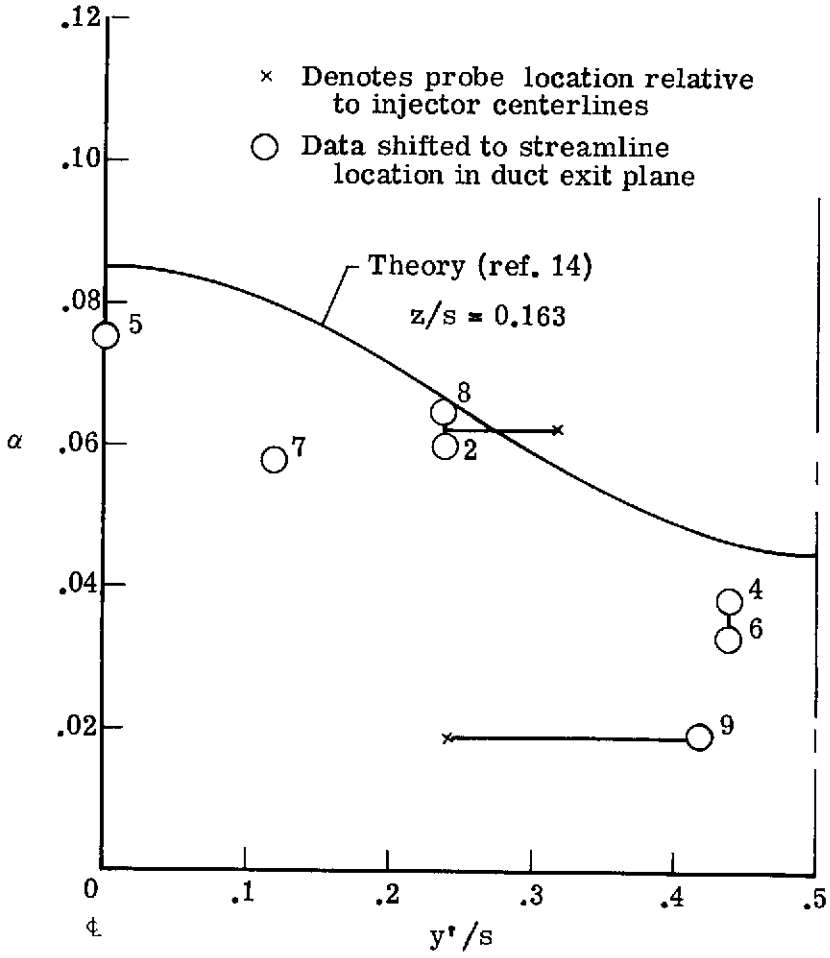

Figure 24.- Parallel injection strut fuel distribution with reaction compared with theory. Run 110-8.

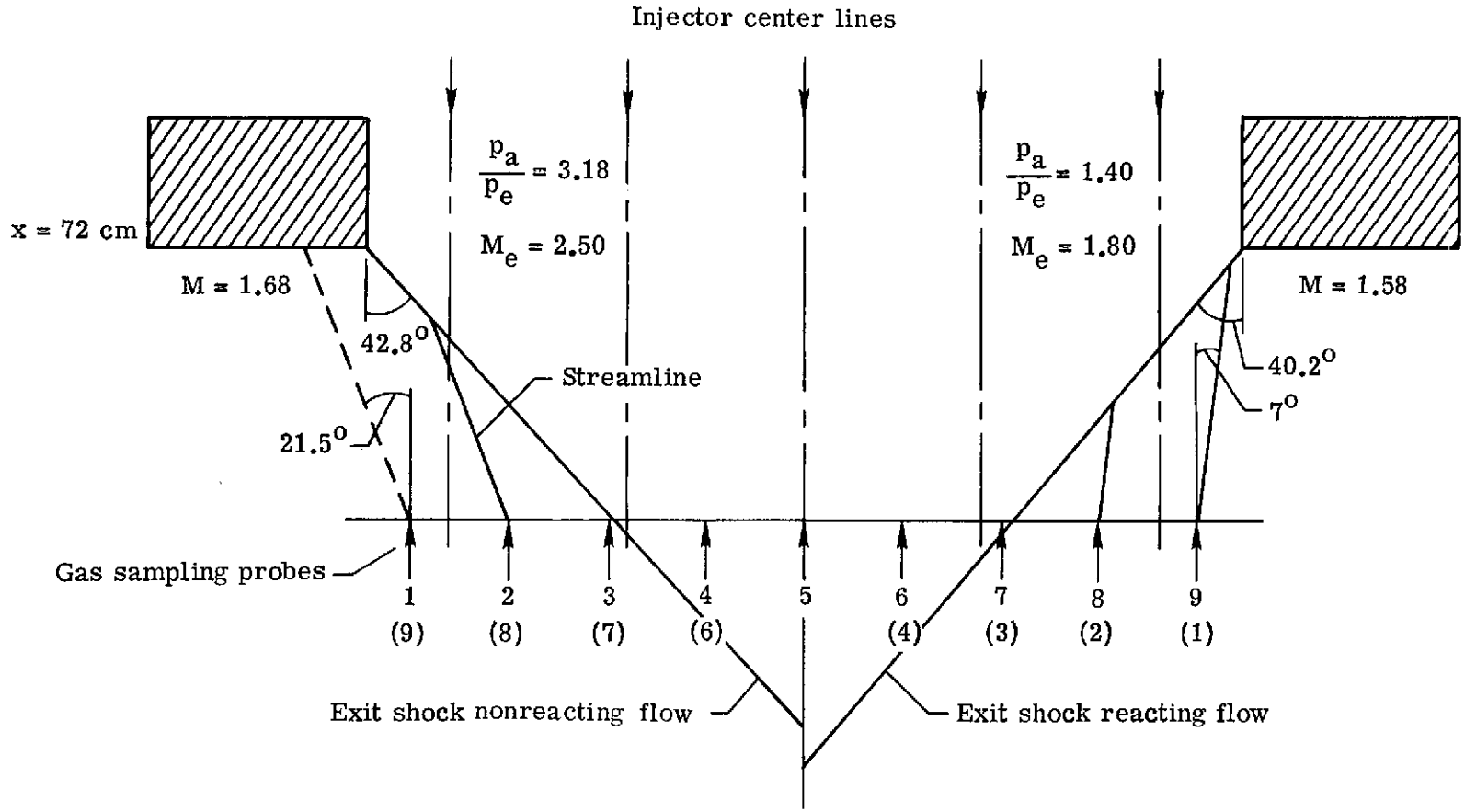

Figure 25.- Duct exit flow model for probe position correction.

CAT-28